A THESIS SUBMITTED TO
THE GRADUATE SCHOOL OF NATURAL AND APPLIED SCIENCES
OF ÇANKIRI KARATEKİN UNIVERSITY

CONTROL OF DOUBLY FED INDUCTION GENERATOR WITH PWM INVERTER

IN PARTIAL FULFILLMENT OF THE REQUIREMENTS
FOR
THE DEGREE OF MASTER OF SCIENCE
IN
ELECTRICAL AND ELECTRONICS ENGINEERING

BY

KANADID ABDI ISMAN

ÇANKIRI

2022

CONTROL OF DOUBLY FED INDUCTION GENERATOR WITH PWM INVERTER

By Kanadid ABDI ISMAN

August 2022

We certify that we have read this thesis and that in our opinion it is fully adequate, in scope and in quality, as a thesis for the degree of Master of Science

Advisor : Assoc. Prof. Dr. Fatih KORKMAZ

Examining Committee Members:

Chairman : Assoc. Prof. Dr. Hayati MAMUR
Electrical and Electronics Engineering
Manisa Celal Bayar University

Member : Assoc. Prof. Dr. Fatih KORKMAZ
Electrical and Electronics Engineering
Çankırı Karatekin University

Member : Asst. Prof. Dr. Göksu GÖREL
Electrical and Electronics Engineering
Çankırı Karatekin University

Approved for the Graduate School of Natural and Applied Sciences

Prof. Dr. İbrahim ÇİFTÇİ
Director of Graduate School

I hereby declare that all information in this document has been obtained and presented in accordance with academic rules and ethical conduct. I also declare that, as required by these rules and conduct, I have fully cited and referenced all material and results that are not original to this work.

Kanadid ABDI ISMAN

ABSTRACT

CONTROL OF DOUBLY FED INDUCTION GENERATOR WITH PWM INVERTER

Kanadid ABDI ISMAN
Master of Science in Electrical and Electronics Engineering
Advisor: Assoc. Prof. Dr. Fatih KORKMAZ

August 2022

The doubly-fed induction generator (DFIG) is based on a wound-rotor induction machine. The stator and the rotor of this induction machine are both connected to an electrical source hence the name doubly fed. In wind energy conversion systems, DFIG with a back-to-back converter is an extensively utilized system. This machine has been the subject of several scientific researches, especially its application in wind energy. This thesis focuses on the control of the Double-Feed Induction Machine by PI Regulator and Fuzzy Logic Regulator Techniques. After presenting the mathematical models of the machine and the converter in the three-phase frame then in the two-phase frame using the Clarke and Park transformations, the vector control of the machine was approached by the orientation of stator flux. A decoupled control of active and reactive power is synthesized employing PI controllers to control the power flowing between the DFIG stator and the grid. Using a fuzzy logic regulator instead of a PI improves overall robustness and tracking performance when dealing with uncertainties. Matlab/SIMULINK software is used to display simulation results for different operating modes.

2022, 84 pages

Keywords: Active power and reactive power control, DFIG, Doubly fed induction generator, Field oriented control, Fuzzy logic controller, PI controller, PWM converter ,Vector control

ÖZET

PWM İNVERTÖR İLE ÇIFT BESLEMELİ ASENKRON JENERATÖRÜNÜN KÖNTROLÜ

Kanadid ABDI ISMAN
Elektrik elektronik Mühendisliği, Yüksek Lisans
Tez Danışmanı: Doç. Dr. Fatih KORKMAZ

Ağustos 2022

Çift beslemeli asenkron jeneratör (ÇBAJ) yapısal olarak, sargılı rotorlu bir asenkron makineye dayanmaktadır. ÇBAJ olarak adlandırılmasının sebebi, statoru ve rotorunun her ikisi de bir elektrik kaynağına bağlı olmasıdır. Rüzgâr enerjisi dönüşüm sistemlerinde, back to back dönüştürücülü ÇBAJ yaygın olarak kullanılmaktadır. Bu özellikleri nedeni ile, ÇBAJ' lerin rüzgâr enerjisine uygulanması da dahil olmak üzere çeşitli bilimsel araştırmalar yapılmıştır. Bu tez, Çift Beslemeli Asenkron Makineyi kontrol etmek için PI ve Bulanık Mantık kontrolörlerinin kullanılmasına odaklanmaktadır. Makinenin ve dönüştürücünün matematiksel modelleri üç fazlı eksende ve ardından Clarke ve Park dönüşümleri kullanılarak iki fazlı eksende tanımlandıktan sonra, makinenin vektör kontrolüne stator akısının yönlendirilmesi ile yaklaşımı denenmiştir. ÇBAJ statoru ile şebeke arasında akan gücü kontrol etmek için PI kontrolörleri kullanılarak aktif ve reaktif gücün ayrıştırılmış denetim yapısı elde edilmiştir. PI yerine bir bulanık mantık kontrolörü kullanılmasıyla, belirsiz koşullar altında genel sağlamlık ve izleme performansı iyileştirilmektedir. Farklı çalışma şartları için simülasyon sonuçları Matlab/SIMULINK programı kullanılarak gösterilmektedir.

2022, 84 sayfa

Anahtar Kelimeler: Aktif ve reaktif güç kontrölü, Bulanık mantık kontrolör, ÇBAJ, Çıft beslemeli asenkron jeneratör, darbe genişlik modülasyonlu dönüştürücü, PI kontrolör, vektör kontrolü

PREFACE AND ACKNOWLEDGEMENTS

I'd like to take this opportunity to express my gratitude to Assoc. Prof. Dr. Fatih KORKMAZ, my advisor, for his patience, understanding, and constant guidance throughout this research project.

Kanadid ABDI ISMAN
Çankırı-2022

CONTENTS

LIST OF SYMBOLS

dq	Park direct and quadrature components
f_r	Rotor frequency
f_s	Stator frequency
I_r	Rotor current
I_s	Stator current
L_s L_r	Stator and rotor inductances
n	Rotor mechanical speed in rpm
n_s	Synchronous speed in rpm
p	Pole pair
R_s R_r	Stator and rotor resistances
s	Slip
V_r	Rotor voltage
V_s	Stator voltage
$\alpha\beta$	Clarke alpha-beta components
ϕ_r	Rotor flux
ϕ_s	Stator flux
θ	Angular position
ω_s	Stator current electrical speed
ω_r	Rotor current electrical speed
ω_m	Rotor electrical speed
Ω_m	Rotor mechanical speed in rad/s

LIST OF ABBREVIATIONS

AC	Alternating current
CDFIG	Cascaded doubly fed induction generator
CW	Control winding
DC	Direct current
DFIG	Doubly fed induction generator
DQ	Direct-quadrature
DSBDFIG	Dual stator brushless doubly fed induction generator
DTC	Direct torque control
FLC	Fuzzy logic controller
FOC	Field oriented control
GSC	Grid side converter
MIMO	Multiple inputs multiple outputs
PI	Proportional integral
PMSG	Permanent magnetic synchronous generator
PW	Power winding
PWM	Pulse width modulation
RSC	Rotor side converter
SC	Scalar vector
SCIG	Squirrel cage induction generator
VC	Vector control
WECS	Wind energy conversion system
WRIG	Wound rotor induction generator

LIST OF FIGURES

LIST OF TABLES

1. INTRODUCTION

This part is an introduction in which we will summarize the research and work carried out by researchers on doubly-fed induction generators, we will set the objective of the thesis and finally the parts of this thesis will be mentioned.

1.1 Introduction

The doubly-fed induction generator is based on a wound rotor induction machine that the windings of both the stator and the rotor can be accessed. The windings of the stator are directly connected to the grid and the windings of the rotor are connected to a back-to-back converter via slip rings and brushes (Şahin 2020). Figure 1.1 shows a doubly fed induction generator in a wind turbine. Its stator and rotor circuits are both connected to the grid. There is a bi-directional AC/DC/AC converter between the grid and the rotor terminals. It is composed of two converters; rotor-side converter and grid-side converter. The role of the grid converter is to regulate the DC-link voltage and to maintain a unity of power factor in rotor power flow. On the other hand with the rotor converter, the active-reactive stator power can be controlled (Ulu and Kömürgöz 2017).

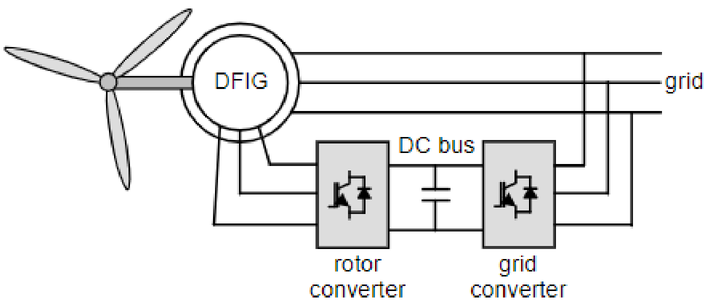

Figure 1.1 DFIG with bidirectional converter in wind turbine system

Only a small portion of the machine's power goes through this converter and the majority of the power of the generator is injected directly into the grid by the stator. The power, the speed and the power factor of the generator can be controlled via this converter. The DFIG is mostly employed in wind turbines because of several advantages such as variable speed generator operation, decoupling between active and reactive power, and low cost (Boubzizi, Abid and Chaabane 2018). Despite the invention of wound-rotor machines by Nikola Tesla in 1888, the use of doubly-fed induction generators in wind energy conversion systems did not become popular until the 1980s after the oil price crisis (Ehlert and Wrede 2007).

1.2 Literature Review

Researchers sought to find an alternative form of energy production that was environmentally friendly and inexpensive. To do this, they have intensified their work on renewable energies. Modernizing these energies presents complexities and requires rigorous control strategies (Moussa, Abdessemed and Benaggoune 2019). Among these renewable energies, there is the wind turbine which has become the most developed renewable energy source in recent decades. This growing technology is impacted by imbalances linked to wind power, such as variable wind speed. To solve this problem, one of the solutions used is the Doubly Fed Induction Generator (DFIG). It is very often deployed in the large wind turbine (Moulay, Habbatti and Hamdaoui, 2019).

As mentioned by (Mwaniki, Lin and Dai 2017), the doubly fed induction generator is one of the four most used machines in the wind energy conversion systems next to the squirrel cage induction generator (SCIG), the Wound Rotor Induction Generator (WRIG) whose rotor is connected to a variable resistor and the Permanent Magnet Synchronous Generator (PMSG). High efficiency even at low wind speed and low initial cost make this machine the most widely used compared to other generators.

The increasing use of this type of machine in wind turbines has led researchers to carry out investigations in order to improve the efficiency of the electromechanical conversion and the quality of the energy supplied.

Dahiya and Leena (2019) compared this machine to the Permanent Magnet Synchronous Generator (PMSG) in wind power conversion systems, as these are the two most widely used types. Their studies on the performance of these two types of generators have shown advantages and disadvantages on both sides. Due to variable speed operation, the DFIG exhibits more power capture and less mechanical stress. But also the capacity of the power electronics is much reduced in the technology using the DFIG compared to that of the Permanent Magnet Synchronous Generator. But also has drawbacks such as the need for a gearbox and slip rings which can be avoided in the other technology since it allows direct-drive systems.

Doubly-fed induction generators can also be used in the conversion of marine energy (tidal energy) where the speed of the currents is also variable like the wind as some researchers made their studies on this. Taking into account the behaviour of the speed of the tidal currents, the DFIG guarantees a good quality of the energy produced by compensating the variations in acceptable proportions (Elghali, Benbouzid and Charpentier 2010).

The double fed induction generator is an induction machine in which the stator and the rotor are powered. The stator circuit is directly connected to the grid and the rotor is connected to the grid using a back-to-back converter. Therefore, 20-25% of the power is exchanged to the grid through this converter (Çalgan 2016).

The use of the doubly-fed induction generator in the production of electricity requires rigorous controls in order to obtain optimum power. The goal being in most cases to bring the slip to the desired value with the best possible efficiency, the rotor windings are supplied by a back-to-back PWM converter which controls certain parameters of the generator. The control of machine speed and flux is most often applied for this system but sometimes other parameters are chosen such as torque, active power and reactive power (Poitiers 2003).

Directly controlling the machine using three-phase signals is very complex for this it is necessary to adopt an adequate strategy. This is possible by applying the transformation of Clarke and Park which makes it possible to pass from a three-phase system to a two-phase system. For this we obtain behaviour similar to that of a direct current motor where the speed and the torque are separately controlled. The generator model is brought into a DQ coordinate which allows manipulating a simple DC signal instead of a complex AC signal (Kılıçaslan 2015).

As to the choice of the controller, there are different methods in the literature; the most used is the classic PI controller (proportional-integral). The proposal of other more sophisticated control methods is developing in the application of DFIG such as sliding mode control, RST and fuzzy supervision control (Bekhada 2015).

1.3 Aim of Thesis

Doubly fed induction generator is a type of machine widely used in power generation in wind energy conversion systems (WECS). It has advantages over other options, such as operating at a slightly lower or higher speed range than the normal rotational speed. This thesis aims to study this type of machine first by modelling it and then by building a control system to regulate the stator active and reactive power. The machine will be controlled by the rotor circuit to obtain desired stator active and reactive power. The rotor side converter and its control will be designed. PI and fuzzy logic controllers will be used and their performance will be studied.

1.4 Thesis Outlines

In this section, the doubly-fed induction generator is described based on researches and the objective of this thesis is mentioned.

The second section examines the structure, different types, and mathematical model of the doubly-fed induction generator. The equations of the machine and the control algorithms are defined.

In the third section, the model of DFIG is developed in Matlab/SIMULINK using the equations describing the generator. The rotor side converter is designed and the control algorithm is implemented in the model to regulate the stator active and reactive power.

In the fourth section, the results of the simulation of DFIG in Matlab are shown. Various simulations are realized to get the results of the machine in different operation modes.

The fifth section is the discussions on the obtained results and summarizes the thesis.

2. DOUBLY FED INDUCTION GENERATOR

2.1 Introduction

A doubly fed induction generator is a machine with two terminals that can be separately connected to external sources. It provides variable speed operation when using in wind energy conversion systems (WECS). Doubly fed induction generators are classified into different types based on their construction. This part concerns the principle of operation of the double-fed induction generator, its different types, and the different control strategies used for the DFIG system.

2.2 Working Principle

Like the classic asynchronous machine, the DFIG consists of two main parts: the stator and the rotor. The stator made up of three windings with sinusoidal distribution, which are the three phases offset by 120 with p pairs of poles. The rotor is also made up of the three windings like the stator. Figure 2.1 shows schematic of two pole pair (p=2) induction machine.

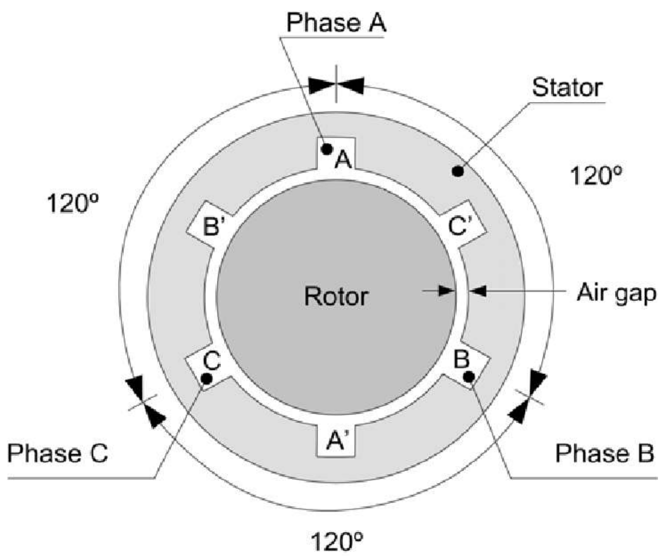

Figure 2.1 Structure of an induction machine with two pole pairs

The stator circuit is directly connected to the grid, imposing the frequency of the stator electrical voltage, whereas the rotor circuit is connected to the grid through converters. The mechanical energy transformed by the machine into electrical energy is fed into the grid mainly through the stator. The rotor can supply or consume energy from the grid so that the machine produces as much energy as possible.

The doubly-fed induction machine can be used as a generator or as a motor; there is no physical difference in their design. In both generating and motoring modes, the machine can operate at a speed lower or higher than the synchronism speed, which is the rotational speed of the magnetic field created by the stator. It is called sub-synchronous operation mode when the machine rotates slower than synchronous speed and super-synchronous operation mode when it rotates faster than synchronous speed (Hlaing 2014). The difference between the rotational speed of the magnetic field of the stator and the rotational speed of the rotor is called slip, given by:

$$\mathbf{s} = \frac{\mathbf{n_s - n}}{\mathbf{n_s}} \tag{2.1}$$

The expressions $\mathrm{s}, \mathrm{n_s}$ and n are the slip, the synchronous speed and the rotational speed of rotor respectively. For a conventional asynchronous machine, the slip is positive in motor mode and negative in generator mode. The induction machine can be described by the Figure 2.2 below which shows the torque-speed characteristic.

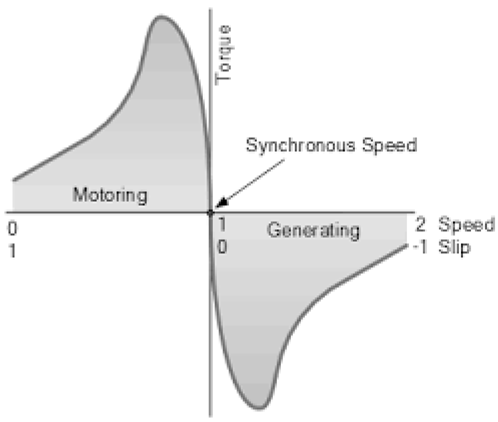

Figure 2.2 Torque-speed characteristic of an induction machine

In the Figure 2.2, we see that the induction machine operates at a speed lower than the synchronous speed when motoring and at a speed higher than the synchronous speed when generating. The slip is between 0 and 1 for a motor and between -1 and 0 for a generator for the classic induction machine. A DFIG can operate at sub-synchronous speed and at super-synchronous speed both in generator mode and in motor mode. DFIG slip varies from -1 to 1 in both modes. The machine can generate electricity when running at a speed below the synchronous speed (Kumar and Choudhary 2014). This can be possible thanks to the circuit of the rotor which can be connected to a source via a bidirectional current converter. This converter allows the power exchanged the rotor and the grid to flow in both ways. The power is fed in and out of the rotor depending on the operating mode. the DFIG can works in four quadrant types of operation which can be distinguished by four different combinations of torque (positive or negative) and speed (sub-synchronous and hyper-synchronous). The torque is negative when the machine working as a generator and positive when working as a motor. The negative means that the machine receives the torque. The slip is negative only in the super-synchronous mode for both the motor and the generator (Abad and Iwanski 2014) .The four quadrant operation of the doubly fed induction machine is illustrated in Figure 2.3.

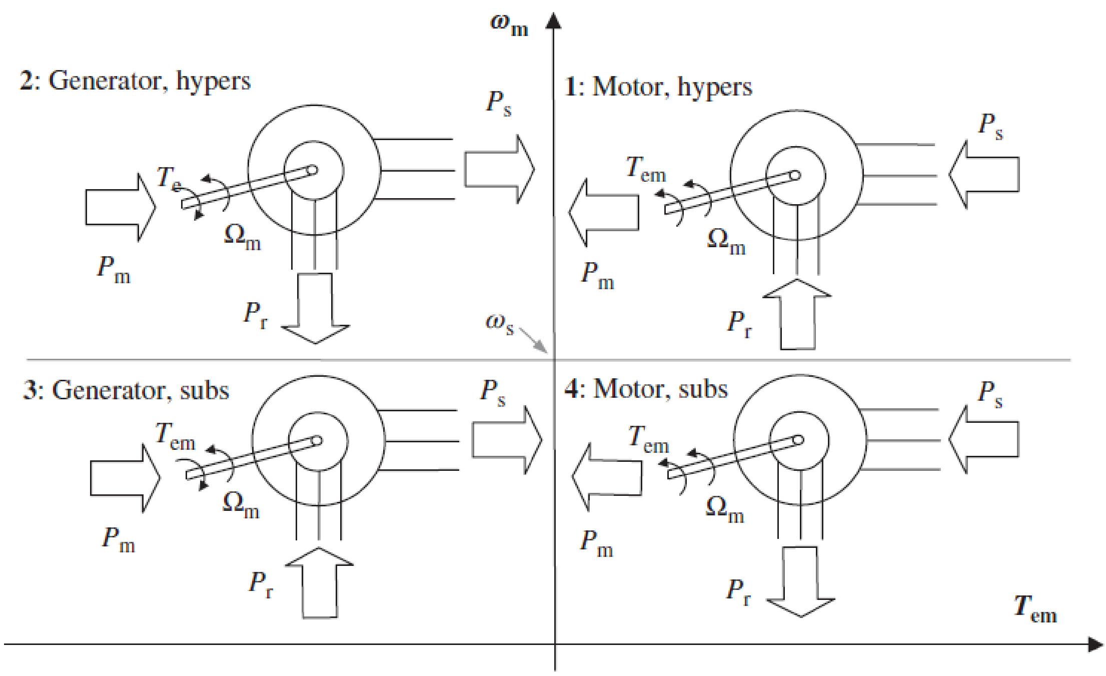

Figure 2.3 Four operating modes of the doubly fed induction machines

There are four operation modes schematised in the figure; they are:

- Motor operation at super synchronism (1); the machine is receiving electric power both in the stator and in the rotor and delivering a mechanical power.
- Motor operation at sub synchronism (4); the stator of the machine is feeding from the grid, but the motor is providing mechanical power and electrical power from the rotor and the shaft of the machine.
- Generator operation at super synchronism (2); the generator is providing electric power from both stator and receiving mechanical power.
- Generator operation at sub synchronism (3); the stator is feeding the power to the grid and the rotor is extracting power from the grid, and the mechanical power is receiving by the generator.

The doubly fed induction machine has also the capability to operate at synchronous speed. The machine is similar to a conventional synchronous machine. The rotor is excited with a DC current (Malik 2015).

2.3 DFIG Types

The double-fed induction machine is an alternative machine that has two accessible three-phase windings that allow the machine to supply or extract energy from a source (Pokharel 2011). There are different types of doubly-fed induction machines. These machines are classified into different categories which are wound rotor types and brushless types (Petersson 2005). The schematic diagrams and descriptions of these machines are as follows:

- Cascaded doubly fed induction generator (CDFIG): It is made up of two asynchronous generators with electrically and mechanically coupled rotors. The stator of one of the two machines is directly connected to the electrical network while the stator of the other is connected to the network through converters which ensure the control of the entire system. Two induction generators are necessary in this design of DFIG called cascaded. It is studied in (Adamowicz and Strzelecki 2008, Tir, Rajeai and Abdessemed. 2010). The schematic of this type of generator is shown in Figure 2.4.

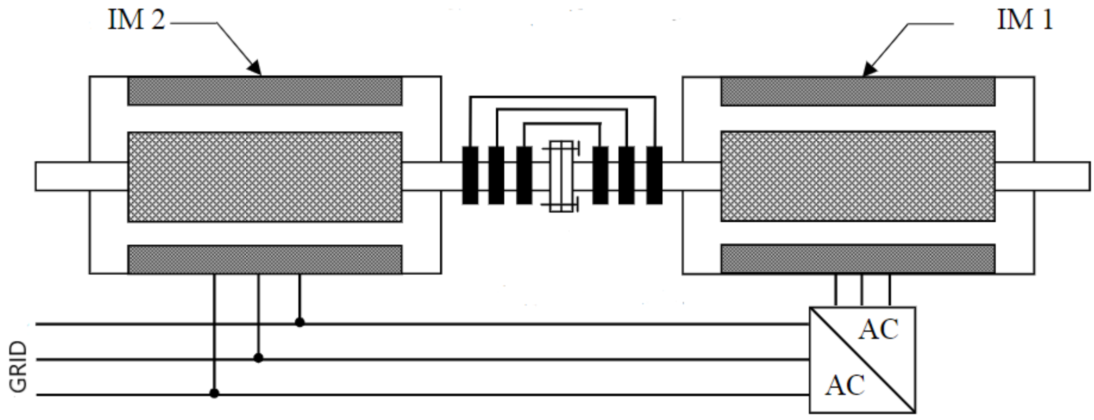

Figure 2.4 Cascaded doubly fed induction machine structure

- Dual stator brushless Doubly Fed Induction Generator (DSBDFIG): Two windings with different numbers of poles are contained in the same stator armature in this sort of machine. One of the windings, called the power winding (PW), is directly connected to the grid and the other winding, called the control winding (CW), is connected to the grid via a converter (Zhang *et al*. 2017, Resmi *et al*. 2015). The Figure 2.5 shows the schematic diagram of this generator.

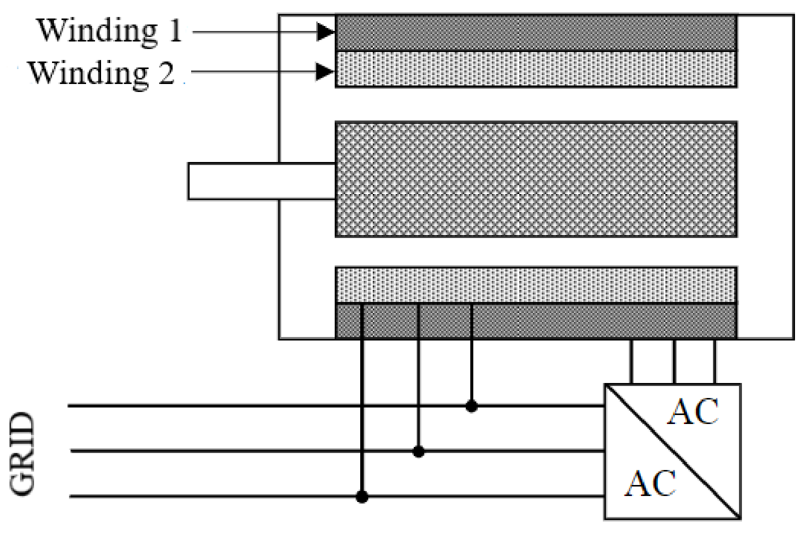

Figure 2.5 Schematic diagram of dual stator doubly fed induction generator

This machine exists in two forms depending on the rotor; one is based on a cage rotor and the other on a variable reluctance rotor. The latter is the most used of this type of machine.

- Doubly fed induction generator based on Wound Rotor Induction Machine (WRIM): this type of generator is the one we are interested in in this thesis. It differs from previous generators because the rotor windings are accessible and are powered by an AC source through bi-directional converters which provide control of the generator while the stator is connected directly to the grid. The Figure 2.6 illustrates the Doubly Fed WRIG.

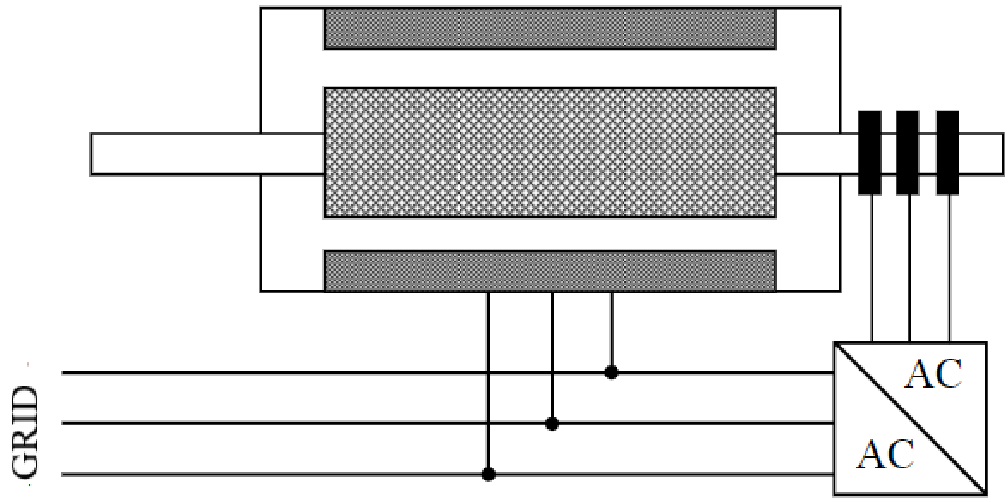

Figure 2.6 Wound rotor induction generator with two accessible windings

The power transiting between the grid and the stator is about 70-80% of the total power of the machine and 20-30% of the power goes through the converter. It is widely used in the electromechanical energy conversion systems. Only this type will be studied in the following sections.

2.4 Control Strategies for DFIG

DFIG is one of the most widely used technologies in variable speed wind energy conversion systems. To improve the technology's performance, a complicated control technique is required. To assure the stability of the system and the quality of the electricity, different control mechanisms are applied to the DFIG. Direct Torque Control (DTC) and Vector Control (VC) are the two main control strategies employed in DFIG control (Khan *et al*. 2020). This two control methods are studied in (Rahmani *et al*. 2015). There are also alternative control strategies for the double fed asynchronous machine that aren't widely used. Only the different control strategies employed for the rotor side converter (RSC) are of interest.

2.4.1 Scalar control

The Scalar Control (SC) approach is used for asynchronous machines because of its simple structure, ease of implementation, and low cost. A constant voltage/frequency (V/f) ratio is maintained in the scalar control method (Ötkün 2020). The machine's supply frequency is modified to achieve variations in speed, while the voltage magnitude is maintained in direct proportion to the applied frequency, ensuring that the machine performs at rated flux. Scalar control has a fundamental coupling effect between torque and flux because both are functions of current and frequency. This strategy is investigated in relation to a double induction generator supplying a disconnected site (Drid, Nait-Said and Makouf 2006). Because of the DFIG, which usually requires more sophisticated controls, the doubly fed induction generator control with scalar control has received less attention in the literature.

2.4.2 Direct torque control

Invented by Takahashi in 1986, direct torque control has become a new technique competing with conventional controls. Because of its high performance and benefits, this technology is commonly used in induction machines (Sahri, Tamalouzt and Belaid 2018). It makes it possible to directly regulate the torque and the flux of the machine. The trajectory and magnitude of the rotor flux can be directly modified using a voltage source converter by injecting different voltage vectors into the rotor of the DFIG. By choosing the best inverter switching states, the flux linkage and the torque of the machine can be directly regulated in the DTC method. Hysteresis controllers keep the flux and torque errors within tolerable limits. The induction machine's DTC may be controlled in a flexible manner and with very quick torque responses (Korkmaz *et al*. 2013). A modulation technique is not used in the DTC strategy. The errors of both torque and flux provide logic outputs. These outputs, and the rotor flux position, are fed to a look-up table, which generates switching action for the voltage source converter (Hassan, El-Sawy and Kamal 2013). Figure 2.7 shows the control of the double-fed asynchronous generator with direct torque control to regulate the torque and rotor fluxes.

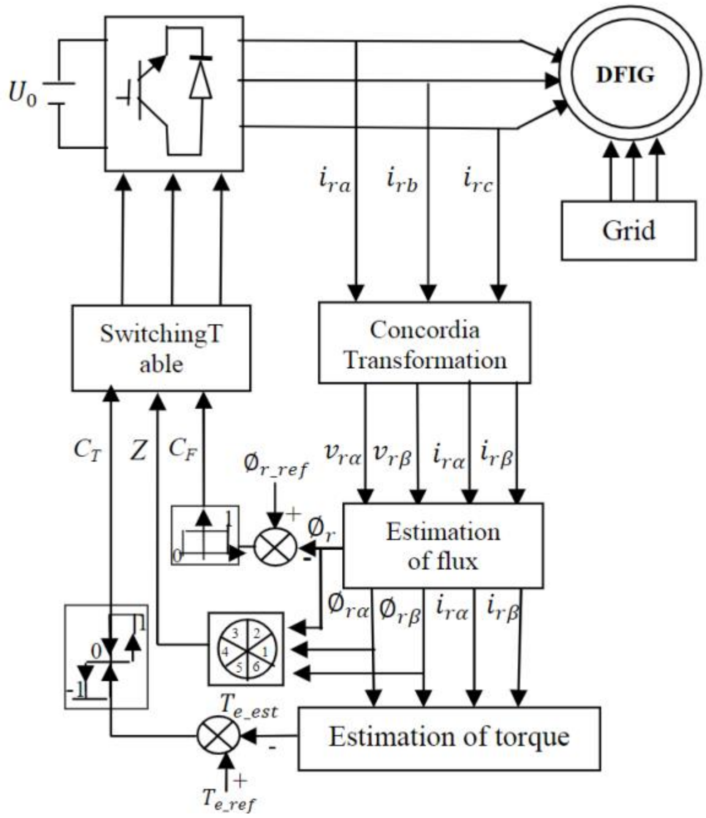

Figure 2.7 DFIG control with direct torque control

2.4.3 Vector control

The vector control also known as field-oriented control (FOC) was introduced by Blaschke and Hasse. The vector control method's fundamental concept is to adopt an appropriate coordinate system to achieve independent torque and flux control. The electromagnetic torque in DC machines is proportional to the product of field current and armature current, while field flux is proportional to field current and unaffected by armature current as shown in Figure 2.8. The purpose of flux orientation is to imitate the behaviour of a separately excited DC machine in a doubly-fed induction machine (El Ouanjli *et al*. 2017). The DFIG is controlled as an independent excitation DC machine with a natural decoupling between the excitation current that produces the flux and the current of a leading that gives electromagnetic torque with vector control (Jenkal *et al*. 2020).

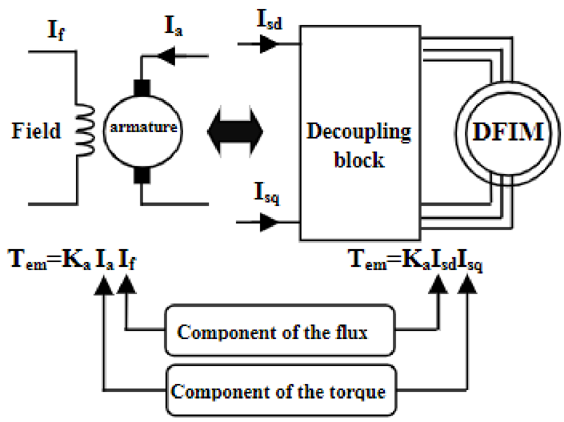

Figure 2.8 Comparison of field oriented control applied to DFIG with DC machine

The FOC method is based on a dynamic study of the machine, which involves transforming a three-phase machine to a rotating two-phase winding equivalent as depicted in Figure 2.9. Clarke and Park transformations are used to change from a time variant three-phase axes coordinate system to a two coordinate rotating reference frame. Clarke transformation modifies the three phase stationary coordinate to a two phase stationary coordinate (Li, Xu and Zhang, 2019). Then Park transformation is applied for purpose to obtain two phase rotating coordinates (d-q).

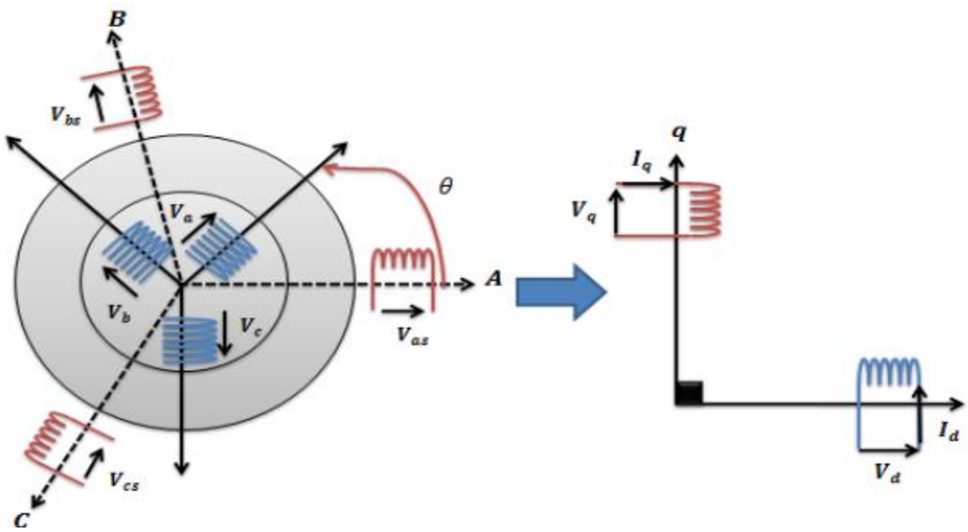

Figure 2.9 Field oriented control for three phase alternative machines

Field oriented control (FOC) can be divided into two categories; direct field oriented control (DFOC) invented by Blaschke and indirect field oriented control (IFOC) presented by Hasse (Kumar and Ramesh, 2015). The rotor angle is measured differently in the two methods. The angle is calculated using terminal voltages and currents in direct FOC, while the angle is calculated using rotor position measurement and machine parameter estimation in indirect FOC. In this thesis, this control strategy will be used to control the stator powers of a grid-connected double-fed induction generator. The necessary transformations and the modelling of the machine will be studied in the following chapter.

3. MODELLING OF DFIG SYSTEM

3.1 Doubly Fed Induction Generator Modelling

The modelling of the doubly-fed induction machine is an essential phase in the design and control of the machine. In this part, the mathematical model of the wound rotor type doubly-fed asynchronous generator will be studied.

3.1.1 Frequencies relations

The relationships between the machine's different frequencies are fundamentals that must be learned before studying the DFIG electric equations. ω_s (Frequency of stator voltages and currents), ω_r (frequency of rotor voltages and currents), and ω_m (rotor electrical speed) are related by the Equation (3.1) (Abad and Iwanski, 2014):

$$\omega_s = \omega_r + \omega_m \tag{3.1}$$

And the relationship between the mechanical speed of the shaft Ω_m and the electrical speed of the machine ω_m is determined by the machine's pole pairs:

$$\omega_m = p\Omega_m \tag{3.2}$$

The difference between the synchronous speed and the rotor electrical speed is determined by the slip s:

$$s = \frac{\omega_s - \omega_m}{\omega_s} = \frac{\omega_r}{\omega_s} \tag{3.3}$$

The relationship between the frequency of stator voltages and the frequency of rotor voltages in Hertz can be deduced:

$$s = \frac{\omega_r}{\omega_s} = \frac{f_r}{f_s} \tag{3.4}$$

$$f_r = sf_s \tag{3.5}$$

The frequency of the currents that must be fed into the rotor is determined by the rotor's rotational speed. The frequency of the rotor currents and voltages f_r become zero when the machine runs at synchronous speed ($s = 0$).

3.1.2 Model in abc-frame

The equivalent circuit of the stator and rotor of a DFIG is shown in Figure 3.1. We assume that the machine's three phases are symmetric, resulting in equivalent self-inductances: $Lsa = Lsb = Lsc$ and $Lra = Lrb = Lrc$. The stator and rotor voltage equations are determined using Kirchhoff's law (Ortatepe, 2020).

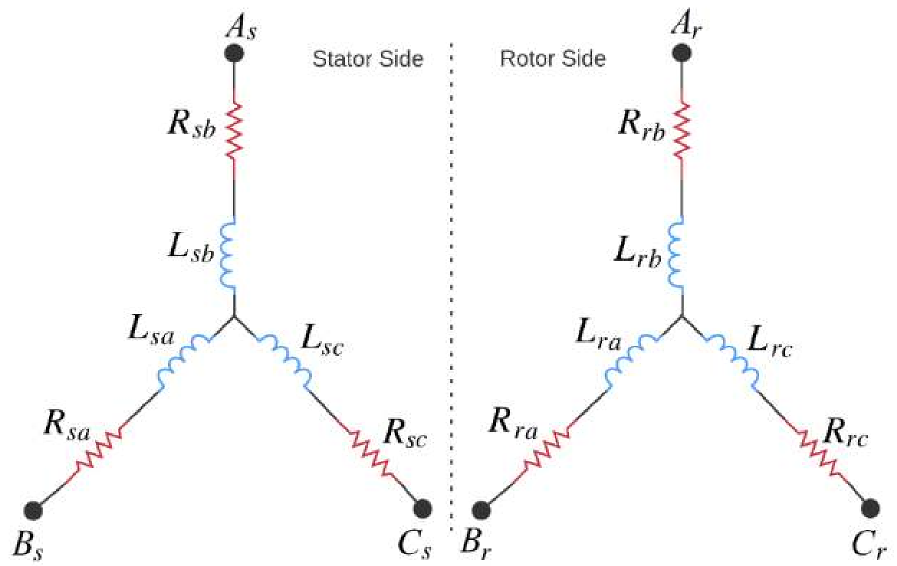

Figure 3.1 Equivalent circuit of doubly fed induction generator

Voltage equations in the DFIG can be written as,

$$V_{sa} = R_{sa}I_{sa} + \frac{d}{dt}\phi_{sa}$$

$$V_{sb} = R_{sb}I_{sb} + \frac{d}{dt}\phi_{sb}$$

$$V_{sc} = R_{sc}I_{sc} + \frac{d}{dt}\phi_{sc}$$

$$V_{ra} = R_{ra}I_{ra} + \frac{d}{dt}\phi_{ra} \quad (3.6)$$

$$V_{rb} = R_{rb}I_{rb} + \frac{d}{dt}\phi_{rb}$$

$$V_{rc} = R_{rc}I_{rc} + \frac{d}{dt}\phi_{rc}$$

V, I and ϕ are representing the voltages, currents and fluxes respectively. The subscripts “s” and “r” are referred to stator and rotor whereas “abc” is for three phase. The flux linkages of machine are expressed as,

$$[\phi_{sabc}] = [L_s] \cdot [I_{sabc}] + [L_{sr}] \cdot [I_{rabc}] \quad (3.7)$$

$$[\phi_{rabc}] = [L_r] \cdot [I_{rabc}] + [L_{rs}] \cdot [I_{sabc}] \quad (3.8)$$

Where,

$$[\phi_{sabc}] = [\phi_{sa} \quad \phi_{sb} \quad \phi_{sc}]^T \quad (3.9)$$

$$[\phi_{rabc}] = [\phi_{ra} \quad \phi_{rb} \quad \phi_{rc}]^T \quad (3.10)$$

And,

$$[I_{sabc}] = [I_{sa} \quad I_{sb} \quad I_{sc}]^T \tag{3.11}$$

$$[I_{rabc}] = [I_{ra} \quad I_{rb} \quad I_{rc}]^T \tag{3.12}$$

The winding inductances can be expressed as (Chouhan 2010),

$$L_s = \begin{bmatrix} l_{ls} + l_m & -\frac{1}{2} l_m & -\frac{1}{2} l_m \\ -\frac{1}{2} l_m & l_{ls} + l_m & -\frac{1}{2} l_m \\ -\frac{1}{2} l_m & -\frac{1}{2} l_m & l_{ls} + l_m \end{bmatrix} \tag{3.13}$$

$$L_r = \begin{bmatrix} l_{lr} + l_m & -\frac{1}{2} l_m & -\frac{1}{2} l_m \\ -\frac{1}{2} l_m & l_{lr} + l_m & -\frac{1}{2} l_m \\ -\frac{1}{2} l_m & -\frac{1}{2} l_m & l_{lr} + l_m \end{bmatrix} \tag{3.14}$$

$$L_{sr} = L_{rs}^T = l_M \begin{bmatrix} cos\theta & \cos(\theta + \frac{2\pi}{3}) & \cos(\theta - \frac{2\pi}{3}) \\ \cos(\theta - \frac{2\pi}{3}) & \cos\theta & \cos(\theta + \frac{2\pi}{3}) \\ \cos(\theta + \frac{2\pi}{3}) & \cos(\theta - \frac{2\pi}{3}) & \cos\theta \end{bmatrix} \tag{3.15}$$

The leakage and magnetizing inductances of the stator windings are expressed by l_{ls} and l_m in the above inductance equations, while the rotor windings are represented by l_{lr} and l_m. The amplitude of the mutual inductances between the stator and rotor windings is represented by l_M. The angle θ is the position of the rotor relative to the stator.

The machine inductances are functions of the rotor position, and the equations that deals with the behaviour of these machines are time varying unless the rotor is at standstill, as shown by the above inductance equations (Kearney, 2013). This dependency can be avoided by transforming the stator and rotor's three-phase variables into a two-axis rotating frame. The Clarke's and Park's transformations are two stages used to achieve this transformation.

3.1.3 Clarke transformations

The Clarke transformation (also known as the αβ transformation) was introduced by Edith Clarke. It describes the transformation of a three-phase system to a two-phase system with a stator-fixed coordinate system (Kainth and Sharma 2014). As shown in the Figure 3.2**,** with the Clarke transformation the balanced three-phase quantities (a, b, c) can be converted into balanced two-phase quadrature quantities (α, β).

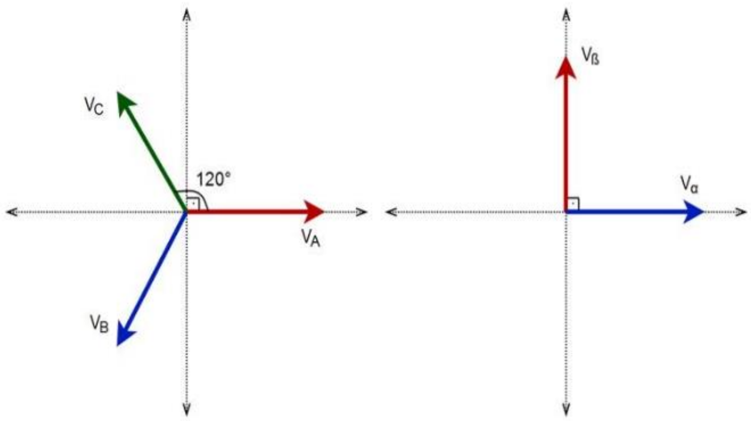

Figure 3.2 Clarke transformation from three phases to two phases

$$\begin{bmatrix} \alpha \\ \beta \end{bmatrix} = C \cdot \begin{bmatrix} a \\ b \\ c \end{bmatrix} \tag{3.16}$$

Where *a*, *b* and *c* are the three-phase system components, *α* and *β* are two-axis system components in orthogonal stationary reference frame. *C* is the simplified Clarke transformation matrix defined by,

$$C = K \cdot \begin{bmatrix} 1 & -\frac{1}{2} & -\frac{1}{2} \\ 0 & \frac{\sqrt{3}}{2} & -\frac{\sqrt{3}}{2} \end{bmatrix} \tag{3.17}$$

For invariant amplitude transformation: $K = \frac{2}{3}$

For invariant power transformation: $K = \sqrt{\frac{2}{3}}$

The Clarke transformation model in Matlab/Simulink tools is shown in Figure 3.3.

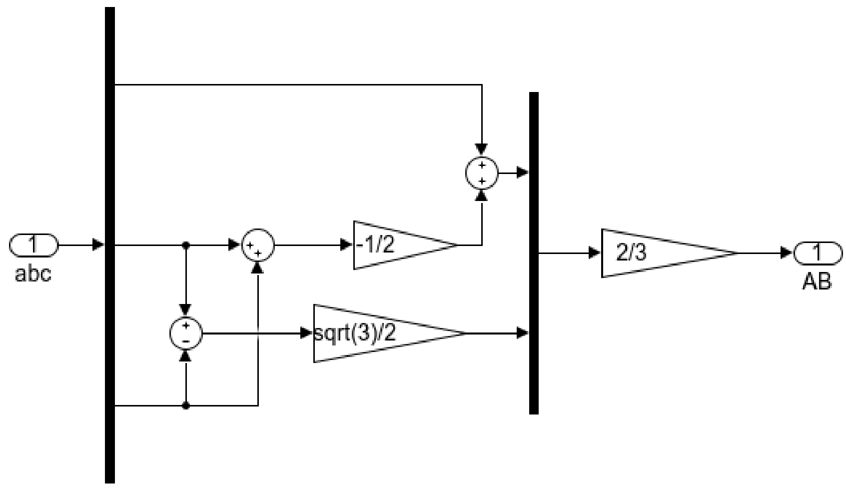

Figure 3.3 Simulink model of Clarke Transform with invariant amplitude

The inverse transformation matrix is:

$$C^T = \frac{1}{K} \cdot \begin{bmatrix} 1 & 0 \\ -\frac{1}{2} & \frac{\sqrt{3}}{2} \\ -\frac{1}{2} & -\frac{\sqrt{3}}{2} \end{bmatrix} \tag{3.18}$$

The three phase reference system quantities can be calculated from the two axis stationary reference frame using the inverse Clarke matrix C^T:

$$\begin{bmatrix} a \\ b \\ c \end{bmatrix} = C^T \cdot \begin{bmatrix} \alpha \\ \beta \end{bmatrix} \tag{3.19}$$

The inverse Clarke transformation model in Matlab/Simulink tools is shown in Figure 3.4.

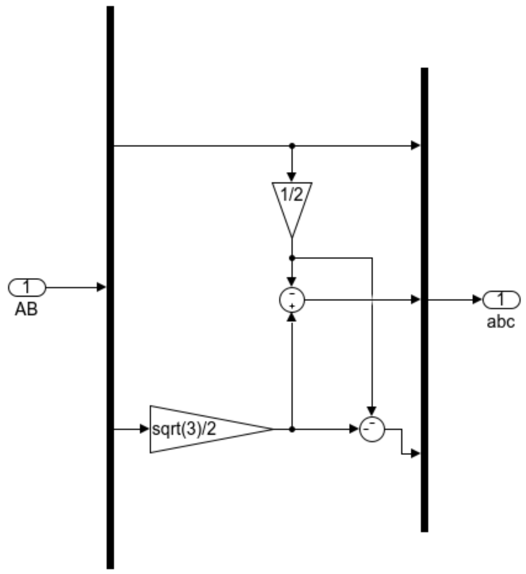

Figure 3.4 Inverse Clarke transform in Simulink

3.1.4 Park transformations

The park's transformation is used to transform two-axis orthogonal stationary reference frame quantities into rotating reference frame quantities (Sunny *et al.* 2016). Also known as the direct-quadrature ($d-q$); the Park transformation was proposed by H. PARK in 1929 (Kumar, Parimi and Rao, 2015). When performing the Park transformation, a stationary 2-phase reference frame obtained using the Clarke transformation can be used as shown in Equation (3.20). The three-phase reference can also be directly translated into the dq reference.

$$\begin{bmatrix} d \\ q \end{bmatrix} = P \cdot \begin{bmatrix} \alpha \\ \beta \end{bmatrix} \tag{3.20}$$

The matrix P is expressed as:

$$P = \begin{bmatrix} cos\theta & sin\theta \\ -sin\theta & cos\theta \end{bmatrix} \tag{3.21}$$

The rotation angle θ is the angle between d axis and α axis and q is perpendicular to d axis as depicted in Figure 3.5.

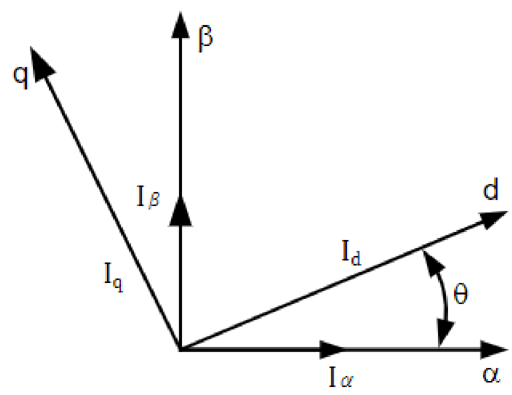

Figure 3.5 αβ to dq transformation

The following is the inverse transformation to transform the quantities from a two-phase rotating to a two-phase stationary frame:

$$\begin{bmatrix} \alpha \\ \beta \end{bmatrix} = P^T \cdot \begin{bmatrix} d \\ q \end{bmatrix} \tag{3.22}$$

$$P^T = \begin{bmatrix} cos\theta & -sin\theta \\ sin\theta & cos\theta \end{bmatrix} \tag{3.23}$$

The Clarke and the Park transformation simplify the analysis of a three-phase system since the waveform of the current and voltage are converted from AC to DC signals. It also makes computations much easier and allows the control of active and reactive power independently. The following Figure 3.6 shows the different references frames (abc, αβ and dq).

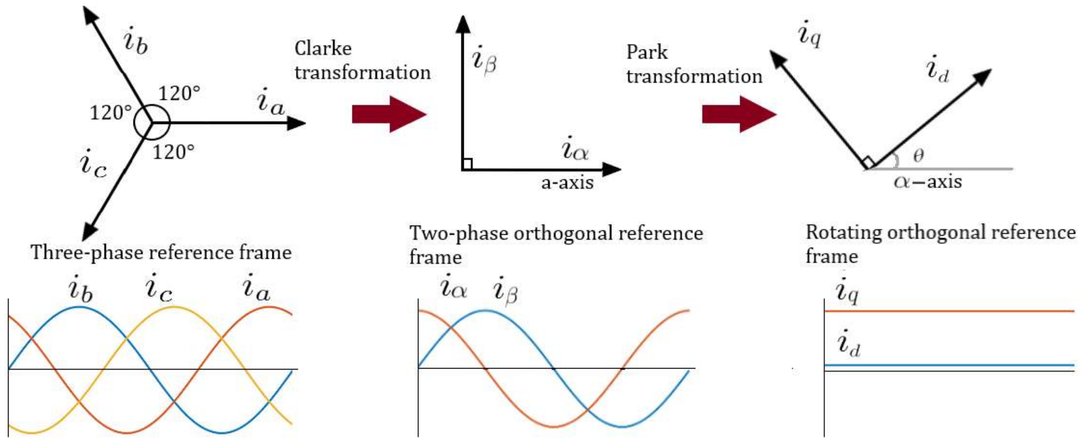

Figure 3.6 Different reference frames with their curves

The park transformation and inverse transformation Simulink blocks are shown in the following Figure 3.7 and Figure 3.8.

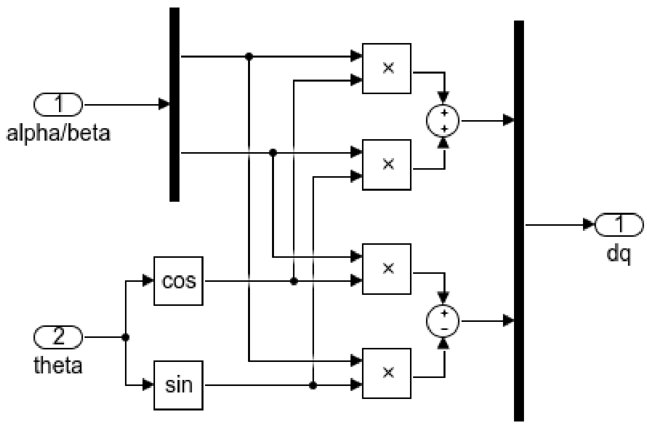

Figure 3.7 Simulink diagram of Park transformation from alpha/beta to dq

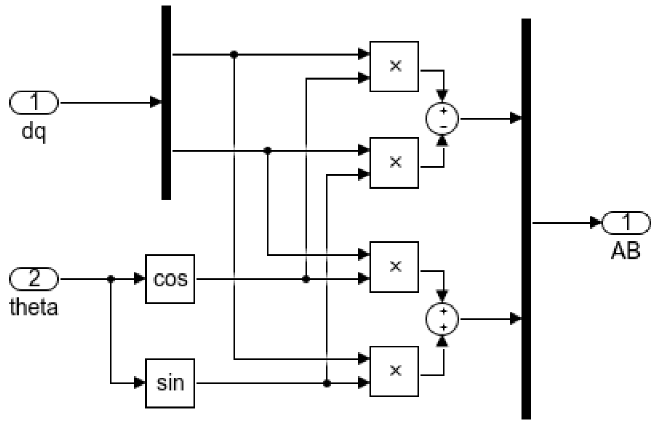

Figure 3.8 Inverse Park transformation from dq to αβ

In the following part, we apply this transformation to the doubly fed induction machine using the previous equations to obtain a dynamic model of this machine.

3.1.5 Dynamic model of doubly fed induction generator

The purpose of this modelling is to find a simple model for the DFIG, allowing passing from three phases to two phases. The basic machine equations are multiplied by the Clarke transformation matrix. The voltages of the generator become in the $\alpha\beta$ reference frame (Ortatepe, 2020):

$$V_{s\alpha} = R_s I_{s\alpha} + \frac{d}{dt}\phi_{s\alpha}$$

$$V_{s\beta} = R_s I_{s\beta} + \frac{d}{dt}\phi_{s\beta} \qquad (3.24)$$

$$V_{r\alpha} = R_r I_{r\alpha} + \frac{d}{dt}\phi_{r\alpha}$$

$$V_{r\beta} = R_r I_{r\beta} + \frac{d}{dt}\phi_{r\beta}$$

These equations are obtaining from the equations given in (3.6) multiply by transformation matrix given in (3.17). The stator and rotor voltages are reduced from three phase to two phase in stationary reference. In the same way, we can get the fluxes equations in the $\alpha\beta$ reference frame:

$$\phi_{s\alpha} = L_s I_{s\alpha} + M[I_{r\alpha}\cos(\theta) - I_{r\beta}\sin(\theta)]$$

$$\phi_{s\beta} = L_s I_{s\beta} + M[I_{r\alpha}\sin(\theta) + I_{r\beta}\cos(\theta)]$$

$$\phi_{r\alpha} = L_r I_{r\alpha} + M[I_{s\alpha}\cos(\theta) + I_{s\beta}\sin(\theta)] \tag{3.25}$$

$$\phi_{r\beta} = L_r I_{r\beta} + M[-I_{s\alpha}\cos(\theta) + I_{s\beta}\sin(\theta)]$$

The stator leakage inductance L_s, rotor leakage inductance L_r and the magnetizing inductance M are calculated as:

$$L_s = l_{ls} + \frac{3}{2} l_m$$

$$L_r = l_{lr} + \frac{3}{2} l_m \tag{3.26}$$

$$M = \frac{3}{2} l_M$$

These inductances are calculated by assuming that the currents that fed the stator and rotor circuits are balanced. Clarke's transformation reduces numbers of dynamic equations. But the stator equations system is represented in stator reference frame, while the rotor equations system is expressed in rotor reference frame, complicating machine analysis. And the mutual inductance is affected by the relative position of the rotor. The main advantage of this model is in real-time applications. Machine analysis must be done when the stator and rotor variables are represented in a common frame of reference. For the purpose to eliminate the time-varying inductances, the park transformation is then applied to the system. With this transformation, the stator and rotor variables are referred to an arbitrary reference frame (dq) which may rotate at any speed ω_e. After that, both the stator and rotor quantities are written in a same frame. The equations of the doubly fed induction machine are written in a common arbitrary reference frame which rotates with angular velocity ω_e (Bayhan, Abu-Rub and Ellabban, 2016):

$$V_{sd} = R_s I_{sd} + \frac{d}{dt}\phi_{sd} - \omega_e \phi_{sq}$$

$$V_{sq} = R_s I_{sq} + \frac{d}{dt}\phi_{sq} + \omega_e \phi_{sd}$$

$$V_{rd} = R_r I_{rd} + \frac{d}{dt}\phi_{rd} - \omega_r \phi_{rq} \qquad (3.27)$$

$$V_{rq} = R_s I_{rq} + \frac{d}{dt}\phi_{rq} - \omega_r \phi_{rd}$$

The above equations are the doubly fed induction generator voltages in Park model. The velocity ω_r is given by $\omega_e - \omega_m$. And the term ω_m is rotor electrical speed.

There are three preferred speeds for ω_e or reference frames as follows (Gupta and Wadhwani 2014):

- The stationary reference frame when the d-q axes do not rotate ($\omega_e = 0$).
- The rotor reference frame when the d-q axes rotate at rotor speed ($\omega_e = \omega_m$).
- The synchronously rotating reference frame when the d-q axes rotate at synchronous speed ($\omega_e = \omega_s$).

The fluxes of the machine in this reference are:

$$\phi_{sd} = L_s I_{sd} + M I_{rd}$$

$$\phi_{sq} = L_s I_{sq} + M I_{rq}$$

$$\phi_{rd} = L_r I_{rd} + M I_{sd} \tag{3.28}$$

$$\phi_{rq} = L_r I_{rq} + M I_{sq}$$

The electromagnetic torque is calculated from the mechanical power divided by the rotor angular velocity and can be expressed in a different ways (Popescu 2000).

$$T_e = \frac{3}{2} p \cdot (\phi_{sd} I_{sq} - \phi_{sq} I_{sd})$$

$$T_e = \frac{3}{2} p \cdot (\phi_{rd} I_{rq} - \phi_{rq} I_{rd}) \tag{3.29}$$

$$T_e = \frac{3}{2} p \cdot M (I_{sq} I_{rd} - I_{sd} I_{rq})$$

Te is the electromagnetic torque, p is number of poles pair of the machine and *M* is the mutual inductance.

The mechanical equation of the generator which represents the relationship between the generator electromagnetic torque and the input mechanical torque is given as:

$$J \cdot \frac{d}{dt} \Omega_m = T_m - T_e - f \cdot \Omega_m \tag{3.30}$$

where *J* the moment of inertia, *f* the viscous coefficient, T_m is the input mechanical torque and represents the prime mover torque and Ω_m is the rotor mechanical speed of the generator. Simulink model of electromagnetic torque calculation from currents is shown in Figure 3.9.

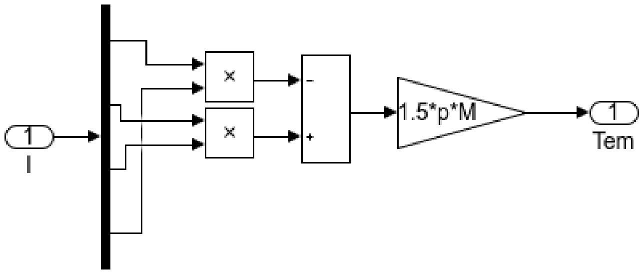

Figure 3.9 Simulink model of electromagnetic torque calculation from currents

3.1.6 State space model of the generator

State-space representations are a simple mathematical methodology for analysing systems with multiple inputs and outputs (MIMO), which are linked by a series of differential and algebraic equations that offer information about the system dynamics (Díaz, González-Morán, and Viescas 2013). The state space representation of the double-fed asynchronous generator can be written as follows (Bekakra, 2010) using Equation (3.27) and Equation (3.28):

$$\frac{d}{dt}\Phi = V - AI - \omega_s CI - \omega_r DI \tag{3.31}$$

The stator and rotor currents are the state variables in this representation. The voltages and the fluxes are the input and the output respectively the state, input, and output vectors are defined as,

$$\Phi = \begin{bmatrix} \phi_{sd} \\ \phi_{sq} \\ \phi_{rd} \\ \phi_{rq} \end{bmatrix} V = \begin{bmatrix} V_{sd} \\ V_{sq} \\ V_{rd} \\ V_{rq} \end{bmatrix} I = \begin{bmatrix} I_{sd} \\ I_{sq} \\ I_{rd} \\ I_{rq} \end{bmatrix} A = \begin{bmatrix} R_s & 0 & 0 & 0 \\ 0 & R_s & 0 & 0 \\ 0 & 0 & R_r & 0 \\ 0 & 0 & 0 & R_r \end{bmatrix}$$

$$C = \begin{bmatrix} 0 & -L_s & 0 & -M \\ L_s & 0 & M & 0 \\ 0 & -M & 0 & -L_r \\ M & 0 & L_r & 0 \end{bmatrix} D = \begin{bmatrix} 0 & 0 & 0 & 0 \\ 0 & 0 & 0 & 0 \\ 0 & M & 0 & L_r \\ -M & 0 & -L_r & 0 \end{bmatrix}$$

The relationship between currents and fluxes is described by Equation (3.28),

$$\begin{bmatrix} \phi_{sd} \\ \phi_{sq} \\ \phi_{rd} \\ \phi_{rq} \end{bmatrix} = \begin{bmatrix} L_s & 0 & M & 0 \\ 0 & L_s & 0 & M \\ M & 0 & L_r & 0 \\ 0 & M & 0 & L_r \end{bmatrix} \begin{bmatrix} I_{sd} \\ I_{sq} \\ I_{rd} \\ I_{rq} \end{bmatrix} \tag{3.32}$$

Using this relation, we can derive the machine's state as a function of only currents and voltages:

$$I = B^{-1} \int (V - AI - \omega_s CI - \omega_r DI) \tag{3.33}$$

This simple equation of state is used to implement the machine's mathematical model in Matlab/Simulink (Figure 3.10).

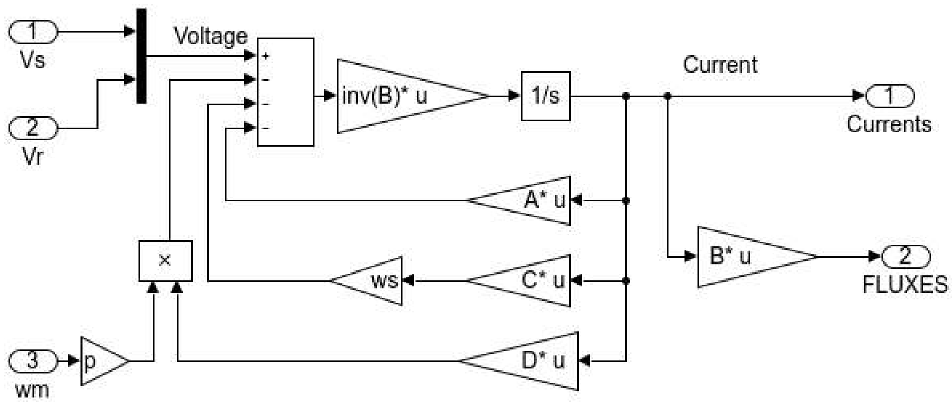

Figure 3.10 Doubly fed induction generator model in Matlab/Simulink

3.2 Modelling of PWM Inverter

3.2.1 Mathematical model of the inverter

DFIG's stator and rotor can both supply power to the grid, the stator is always feeding the grid, but the direction of power flow through the rotor circuit is determined by the generator's speed. The stator windings are directly connected to the grid, whereas the rotor windings use slip rings and voltage source converter to connect to the grid. With only 30% of the machine's power, this converter is a back-to-back voltage source converter (Amorim, Oliveira and Simonetti 2021). The rotor power flow from and to the generator is controlled by this power electronic. This power electronic consists of two bidirectional AC/DC converter named rotor side converter (RSC) and grid side converter (GSC). The rotor side converter's purpose is to control active and reactive power flows at the stator. And the grid side converter's role is to maintain a constant DC link voltage independent of the magnitude and direction of the rotor power. In this work, only the rotor side converter will be designed and the DC link and the grid side converter will be replaced by DC voltage source.

The rotor side converter is a voltage source converter that can work as both a rectifier and an inverter. There are a variety of three-phase VSI circuit topologies, this thesis focuses on the conventional two-level three-phase VSI depicted in the following figure.

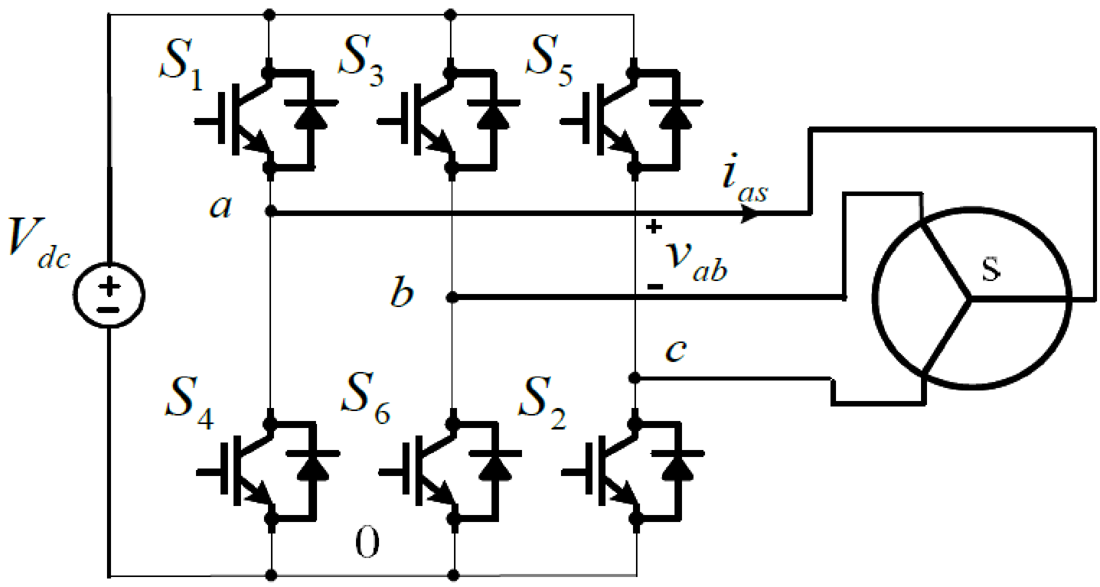

Figure 3.11 Voltage source inverter

Figure 3.11 depicts a two-level three-phase voltage source inverter (VSI) with six switches, S_1 to S_6, and a dc constant voltage source Vdc connected to a three-phase load. The power devices in this inverter are considered ideal switches. This bidirectional AC-DC converter has two modes of operation. In rectifier mode, the bidirectional AC-DC converter acts as a front end rectifier, allowing power to be transferred from the three-phase AC voltage end to the DC voltage bus. The second mode is inverter mode, in which power is transferred from the DC voltage bus to the three-phase AC voltage end of the converter, which operates as a voltage source inverter. To allow bidirectional current flow in each phase-leg, and hence bidirectional power flow between the ac and dc sides, the VSC employs composite self-commutated switching devices such as the insulated gate bipolar transistor (IGBT) (Akter *et al*. 2015).

To develop the mathematical model of this inverter, the Kirchhoff voltage law is applied to the converter.

$$V_{as} = V_{ao} - V_{so}$$

$$V_{bs} = V_{bo} - V_{so} \quad (3.34)$$

$$V_{cs} = V_{co} - V_{so}$$

Where V_{as}, V_{as}, and V_{cs} are the phase-to-neutral voltages.

The sum of these three voltages is:

$$V_{as} + V_{bs} + V_{cs} = V_{ao} + V_{bo} + V_{co} - 3V_{so} \qquad (3.35)$$

Assuming that the load is balanced, we have:

$$V_{as} + V_{bs} + V_{cs} = 0$$

$$V_{so} = \frac{1}{3}(V_{ao} + V_{bo} + V_{co}) \qquad (3.36)$$

The mathematical model of the inverter is then obtained by using these expressions:

$$V_{as} = \frac{1}{3}(2V_{ao} - V_{bo} - V_{co})$$

$$V_{bs} = \frac{1}{3}(-V_{ao} + 2V_{bo} - V_{co}) \qquad (3.37)$$

$$V_{cs} = \frac{1}{3}(-V_{ao} - V_{bo} + 2V_{co})$$

And

$$V_{ao} = S_a \cdot V_{dc}$$

$$V_{bo} = S_b \cdot V_{dc} \qquad (3.38)$$

$V_{co} = S_c \cdot V_{dc}$

In the equations S_a, S_b and S_c are three phase switching state functions of the inverter and are determined as follows:

$$S_a = \begin{cases} 1, & if\ S_1 is\ ON\ and\ S_4 is\ OFF \\ 0, & if\ S_1 is\ OFF\ and\ S_4 is\ ON \end{cases}$$

$$S_b = \begin{cases} 1, & if\ S_3 is\ ON\ and\ S_6 is\ OFF \\ 0, & if\ S_3 is\ OFF\ and\ S_6 is\ ON \end{cases}$$

$$S_c = \begin{cases} 1, & if\ S_5 is\ ON\ and\ S_2 is\ OFF \\ 0, & if\ S_5 is\ OFF\ and\ S_2 is\ ON \end{cases}$$

The switching functions are square waveforms that take 0 for certain intervals of time during each fundamental period and 1 for the rest of the fundamental period. After using the dc bus voltage Vdc and the switching state functions, the voltage on the ac side of the inverter becomes (Mahboub 2018),

$$V_{as} = \frac{V_{dc}}{3}(2S_a - S_b - S_c)$$

$$V_{bs} = \frac{V_{dc}}{3}(-S_a + 2S_b - S_c) \tag{3.39}$$

$$V_{cs} = \frac{V_{dc}}{3}(-S_a - S_b + 2S_c)$$

These equations are representing the mathematical model of the three phase voltage source inverter. According to this mathematical representation, any modulation strategy is possible. This contribution's proposed model is based on the Pulse Width Modulation (PWM) method, in which the switches in each leg of the inverter are turned on and off at a high frequency.

3.3 Pulse Width Modulation

Pulse width modulation is a technology used to control semiconductor devices in power electronics. PWM is a common control method for generating analog signals from digital devices (Cho *et al*. 2007). Inverter control utilizes a variety of modulation techniques. Some of these techniques can be used digitally, while others can be used analogously. Sinusoidal PWM and space vector PWM are the most extensively utilized techniques. The Sinusoidal Pulse Width Modulation (SPWM) technique was adopted to control the inverter in this design since the output voltage and frequency of the inverter can be directly controlled using sine functions.

Three sinusoidal reference waves, each displaced by 120°, are used in three-phase inverter SPWM. To generate the gating signals for a phase, a carrier wave is compared to the reference signal corresponding to that phase. The modulated pulse's switching instants and commutation are determined by the junction of carrier signal with high frequency and reference signal with low frequency waves. When the reference sinusoidal signals exceed the carrier triangular wave, the switching devices will turn on. The comparison of sine and triangle wave waveforms, as well as pulse generation, is depicted in Figure 3.12.

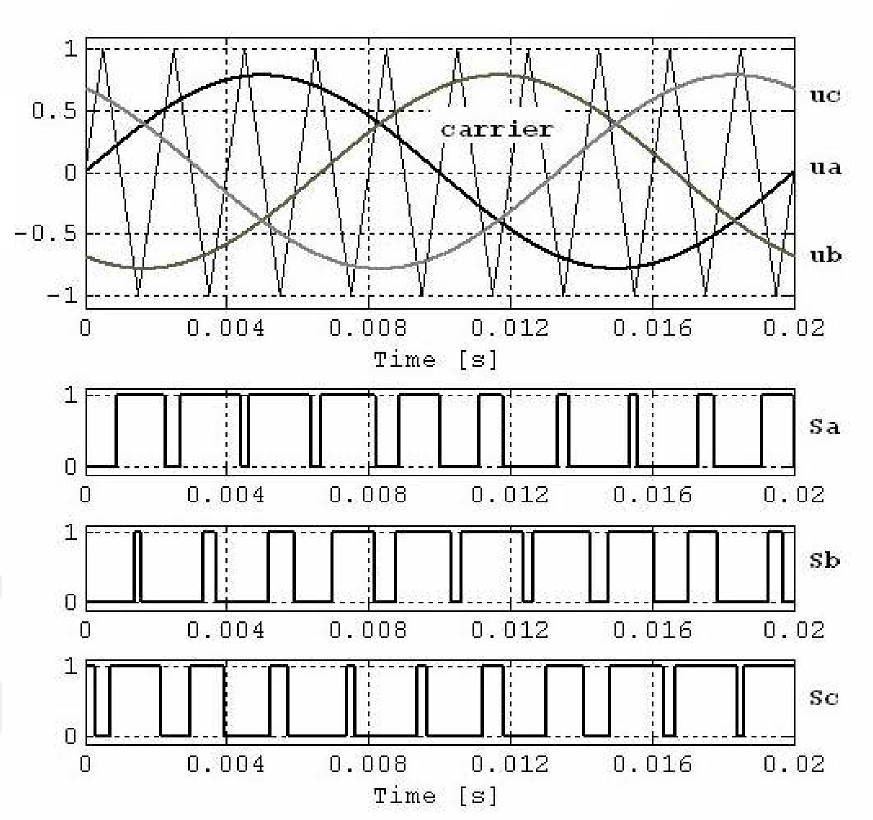

Figure 3.12 PWM technique signals; carrier signal (triangular), modulation signal (sinusoidal) and switching function (square).

The reference voltage signals Ua, Ub, and Uc are usually sinusoidal of the required output frequency, as shown in the diagram. These signals are called the modulating signals. The triangle signal is the carrier with hundredfold higher than the frequency of reference signals. Sa, Sb and Sc are switching state signals used for inverter switches.

The frequency modulation rate (m_f) is expressed as the ratio of the carrier wave frequency to the control signal frequency (Mahboub 2018).

$$m_f = \frac{f_{carrier}}{f_{reference}} \quad (3.40)$$

The terms m_f, $f_{carrier}$ and $f_{reference}$ are frequency ratio, carrier signal frequency and reference signal frequency respectively.

The amplitude modulation ratio (m_a) or modulation index is the ratio of the reference wave amplitude to the triangle wave amplitude.

$$m_a = \frac{V_{reference}}{V_{carrier}} \tag{3.41}$$

m_a, $V_{carrier}$ and $V_{reference}$ are amplitude index, carrier signal amplitude and reference signal amplitude respectively. The effective value of the output voltage in PWM inverters is determined by the modulation index magnitude.

The reference signals are generated by the control system of the generator, which will be discussed in the next section.

3.4 Dynamic Model of PWM Inverter

Although the three phase frame's PWM voltage source converter model has straightforward meanings, all of the components in the abc model are time variable, causing problems and challenges in controller design. As a result, the abc model must be transformed to a DQ model that rotates at synchronous speed in order for the three-phase voltage inputs and current components to be converted to constant values (Raju and Raju 2015). To do this the Clarke and Park transformations used previously for the generator are employed. When the converter is connected to the machine's rotor, the following equation can be written:

$$\frac{V_{dc}}{3}(2S_a - S_b - S_c) = R_{ra}I_{ra} + \frac{d}{dt}\phi_{ra}$$

$$\frac{V_{dc}}{3}(-S_a + 2S_b - S_c) = R_{rb}I_{rb} + \frac{d}{dt}\phi_{rb} \tag{3.42}$$

$$\frac{V_{dc}}{3}(-S_a - S_b + 2S_c) = R_{rc}I_{rc} + \frac{d}{dt}\phi_{rc}$$

The dynamic model of the converter is obtained using Clarke and Park transformations:

$$S_d \cdot V_{dc} = R_r I_{rd} + \frac{d}{dt}\phi_{rd} - \omega_r \phi_{rq}$$

$$S_q \cdot V_{dc} = R_r I_{rq} + \frac{d}{dt}\phi_{rq} - \omega_r \phi_{rd} \quad (3.43)$$

Where *Ird* and *Irq* are the rotor currents, Vdc is the DC bus voltage ϕrd *and* ϕrq are currents fluxes. *Sd* and S_q are switching state functions in dq reference frame. The switches function contains high harmonics generated during the PWM switching. If these harmonics are neglected, the following expression can be written (Hussien and Hassan 2019):

$$S_d \cdot V_{dc} = \mathrm{V_{rd}}$$

$$S_q \cdot V_{dc} = \mathrm{V_{rq}} \quad (3.44)$$

4. FIELD ORIENTED CONTROL ON DFIG

The control of the doubly-fed induction generator is explored in this section, and the stator flux orientation is applied to the machine to control the generator's real and reactive powers with the rotor side inverter modelled in the previous chapter. The PI regulator and the fuzzy logic regulator have been developed for power regulation.

4.1 Stator Field Orientation

The stator-flux oriented frame is the most commonly utilized frame for the design and analysis of DFIG. In this frame, the rotor currents' q-axis and d-axis components are used for active and reactive power control, respectively (Sarma *et al*. 2018). As depicted in Figure 4.1 the d-axis of the Park reference frame is aligned with the stator-flux in the stator-flux orientation frame, implying that the q-axis flux linkage is 0 and the d-axis flux linkage is constant (Jenkal *et al*. 2020, Radaideh, Bodoor, and Al-Quraan 2021).

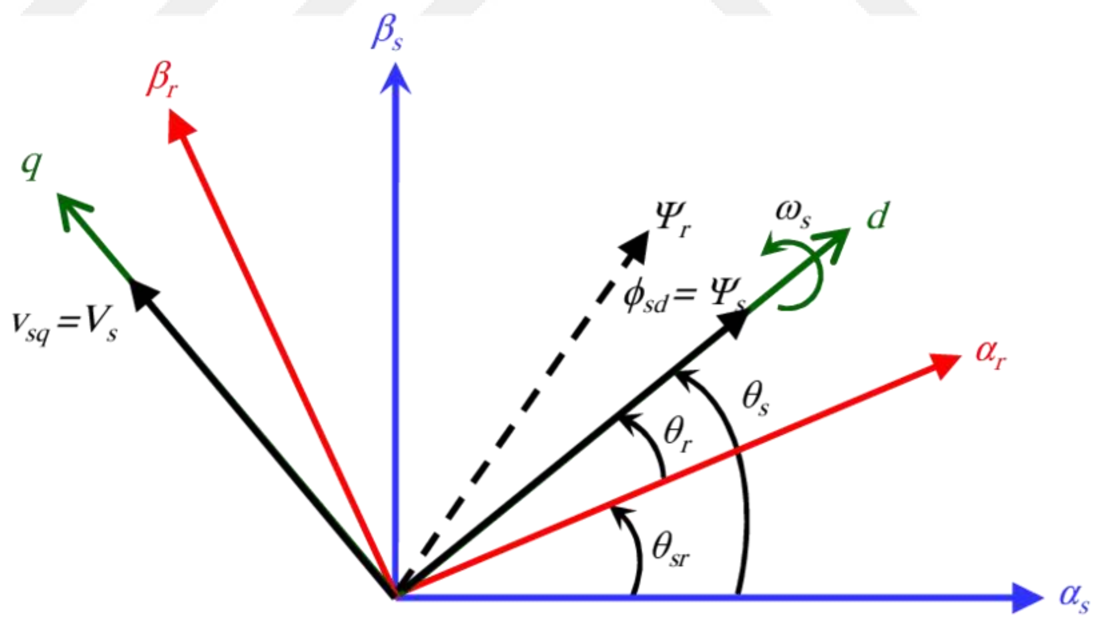

Figure 4.1 Stator field oriented control technique**.**

Since the stator is directly connected to the grid and the stator flux can be considered constant, one can write:

$$\phi_{sd} = \Phi_s \; and \; \phi_{sq} = 0 \tag{4.1}$$

ϕ_s is the amplitude of the stator flux.

The relation between stator voltages and stator fluxes in Equation (3.27) is applicable in this new frame. The stator voltage in the stator flux orientation reference frame is:

$$V_{sd} = 0 \; and \; V_{sq} = V_s = \Phi_s \omega_s \tag{4.2}$$

V_s is the amplitude of the stator voltage.

The stator flux in Equation (3.28) becomes:

$$\phi_{sd} = \Phi_s = L_s I_{sd} + M I_{rd}$$

$$\phi_{sq} = 0 = L_s I_{sq} + M I_{rq} \tag{4.3}$$

From this relation, one can determine the relation between the stator and rotor currents:

$$I_{sd} = \frac{\Phi_s}{L_s} - \frac{M}{L_s} I_{rd}$$

$$I_{sq} = -\frac{M}{L_s} I_{rq} \tag{4.4}$$

From this relation the rotor fluxes are calculated:

$$\phi_{rd} = \sigma L_r I_{rd} + \frac{M \Phi_s}{L_s}$$

$$\phi_{rq} = \sigma L_r I_{rq} \tag{4.5}$$

σ is called the leakage factor and defining as:

$$\sigma = 1 - \frac{M^2}{L_r L_s} \tag{4.6}$$

In the stator flux orientation frame, the above equations describe the doubly-fed induction generator. The active and reactive powers in the stator windings can be calculated in the stator field orientation reference:

$$P_s = \frac{3}{2}(V_{sd}I_{sd} + V_{sq}I_{sq})$$

$$Q_s = \frac{3}{2}(V_{sq}I_{sd} - V_{sd}I_{sq}) \tag{4.7}$$

Taking into consideration the fact that *Vsd* is equal to zero in Equation (4.2), on can obtain the following expressions.

$$P_s = \frac{3}{2}V_{sq}I_{sq}$$

$$Q_s = \frac{3}{2}V_{sq}I_{sd} \tag{4.8}$$

As shown in Equation (4.5), the rotor and stator currents have a linear relationship. If the stator currents are substituted by their terms, we get (Bakır, Merabet and Kulaksız 2020):

$$P_s = -\frac{3}{2}\frac{MV_s}{L_s}I_{rq}$$

$$Q_s = -\frac{3}{2}\frac{MV_s}{L_s}I_{rd} + \frac{3}{2}\frac{V_s^2}{L_s\omega_s} \tag{4.9}$$

This relation shows that the control of stator active and reactive power can be realized by controlling the rotor current (Eltamaly, Al-Saud and Abo-Khalil 2020).

Figure 4.2 illustrate the stator power calculation block using the stator voltage and current.

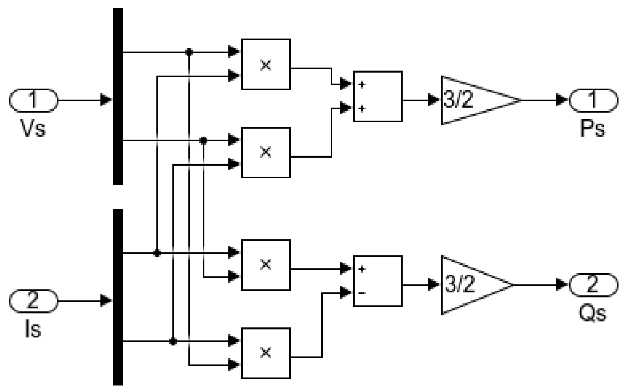

Figure 4.2 Stator powers calculation block in Matlab/Simulink.

4.2 Power Control Method

The active and reactive powers of the machine are controlled by the rotor side converter (Behara and Behara 2022). The relationships between stator powers and rotor voltages defined above are employed to accomplish this control. The stator active and reactive powers are controlled by Iqr and Idr, respectively. We could express the rotor voltages in terms of rotor currents:

$$V_{rd} = R_r I_{rd} + \sigma L_r \frac{d}{dt} I_{rd} - \omega_{slip} \sigma L_r I_{rq}$$

$$V_{rq} = R_r I_{rq} + \sigma L_r \frac{d}{dt} I_{rq} + \omega_{slip}(\sigma L_r I_{rq} + \frac{M V_s}{L_s \omega_s}) \tag{4.10}$$

The angular slip speed is: $\omega_{slip} = \omega_s - \omega_m$

The above equations form the basis of the controller designed to control stator powers and are directly used for this purpose. These equations can be written as the sum of two terms as follows:

$$V_{rd} = V_{rd}^{*} + E_{rd}$$

$$V_{rq} = V_{rq}^{*} + E_{rq} \tag{4.11}$$

Where,

$$V_{rd}^{*} = R_r I_{rd} + \sigma L_r \frac{d}{dt} I_{rd}$$

$$V_{rq}^{*} = R_r I_{rq} + \sigma L_r \frac{d}{dt} I_{rq} \tag{4.12}$$

And,

$$E_{rd} = -\omega_{slip} \sigma L_r I_{rq}$$

$$E_{rq} = \omega_{slip} (\sigma L_r I_{rq} + \frac{M V_s}{L_s \omega_s}) \tag{4.13}$$

V_{rd}^{*} and V_{rq}^{*} are considered to be the state equation between the voltage and current in d and q loops of the controller. E_{rd} and E_{rq} are the compensating elements of the equation.

4.3 PI Controller Design

The PI controller is a feedback control loop that is extensively employed in industrial control systems (Bharti, Saket and Nagar 2018). The rotor side converter allows independent control of the stator's reactive and active powers. Figure 4.3 provides an illustration of the control loop. The rotor current is decomposed into an active power (q-axis) and a reactive power (d-axis) component since the converter performs in a stator-flux dq-reference frame.

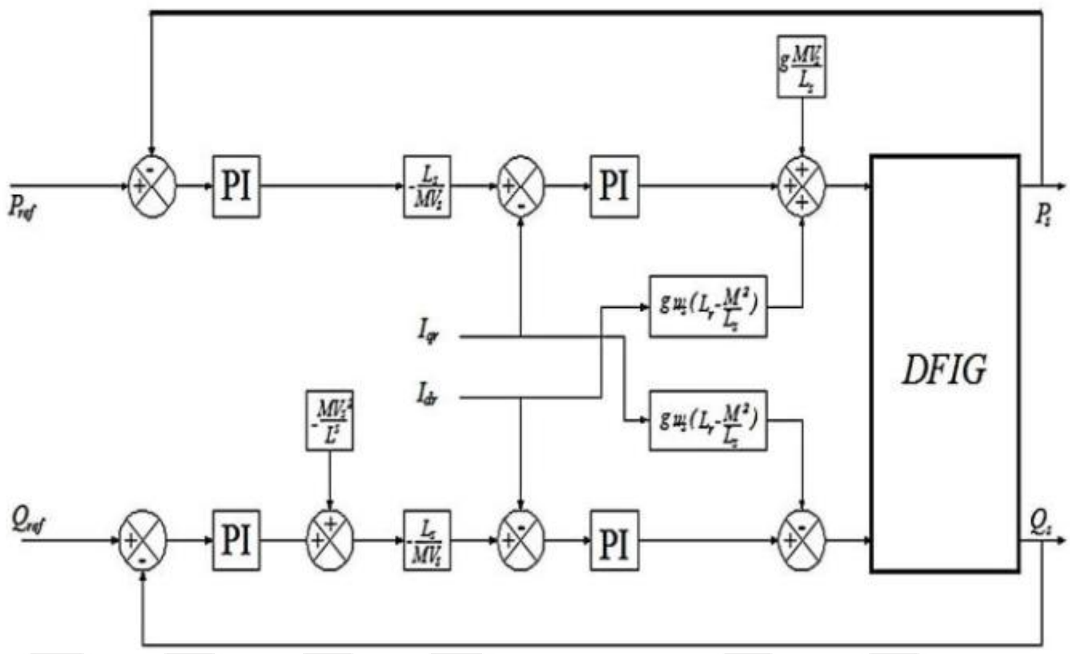

Figure 4.3 DFIG Power Control scheme

As shown in Figure 4.3, the generator's real active power is compared to a reference point value. The difference between these two values is fed into a Proportional Integral (PI) controller, which generates the required q-axis rotor current value. Similarly, a reactive power side PI controller is used to generate the required d-axis rotor current. The rotor currents are controlled by two additional PI controllers. At the output of these two regulators, we have the desired rotor voltages that will be injected into the generator's rotor. These controllers are used to independently control the active and reactive power outputs, and they are organized in two cascaded loops, with two PI controllers in each control loop. In this type of control, two regulators are set up for rotor currents and two for stator powers.

4.3.1 Tuning of PI current controllers

The block diagram in Figure 4.4 depicts the rotor current regulation loops. The d-q components of the rotor current transfer functions are obtained using Equation (4.12):

$$\frac{I_{rd}}{V_{rd}^*} = \frac{1}{R_r + \sigma L_r p} \quad and \quad \frac{I_{rq}}{V_{rq}^*} = \frac{1}{R_r + \sigma L_r p} \tag{4.14}$$

The current function transfers for the direct and quadrature axes are same. As a result, the PI regulators designed for currents will have equal gains.

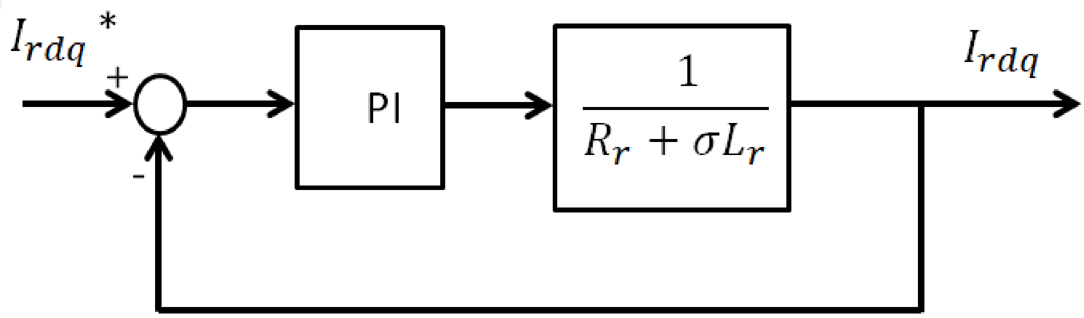

Figure 4.4 Current regulation diagram I_{rd} and I_{rq}

The PI controllers are simple and can eliminate steady-state error. Its transfer function is as follow:

$$PI(p) = K_p + \frac{K_i}{p} \tag{4.15}$$

The open loop transfer function (OLTF) of the diagram in Figure 4.4 can be written as follows.

$$OLTF(p) = \frac{K_i}{p}\left(p\frac{K_p}{K_i} + 1\right)\frac{1}{R_r\left(1 + p\frac{\sigma L_r}{R_r}\right)} \tag{4.16}$$

The compensation method is applied for the synthesis of the regulator poles in order to eliminate the zero of the transfer function (Hamane *et al*. 2014). This results in:

$$\frac{K_p}{k_i} = \frac{\sigma L_r}{R_r} \tag{4.17}$$

We obtain the following OLTF by performing the compensation:

$$OLTF(p) = \frac{K_i}{pR_r} \tag{4.18}$$

This equation gives us a closed loop transfer function CLTF:

$$CLTF(p) = \frac{1}{(1+p\tau_r)} \tag{4.19}$$

With: $\tau_r = \frac{R_r}{K_i}$

The system response time is τ_r.

The gains of the Correctors can be represented in machine parameters and response time as follows:

$$K_p = \frac{\sigma L_r}{\tau_r}$$

$$K_i = \frac{R_r}{\tau_r} \tag{4.20}$$

Because of its rapidity, the pole compensation method was used; however, it is obvious that this is not the only viable method for tuning the PI regulator.

4.3.2 Tuning of PI power controllers

A PI regulator is designed to ensure that the DFIG's active and reactive powers follow their reference values. The PI regulator's purpose is to improve robustness against internal and external perturbations. As with rotor currents, active and reactive power provides the same transfer function. The block diagram in Figure 4.5 depicts the active Ps and reactive Qs power regulation loops.

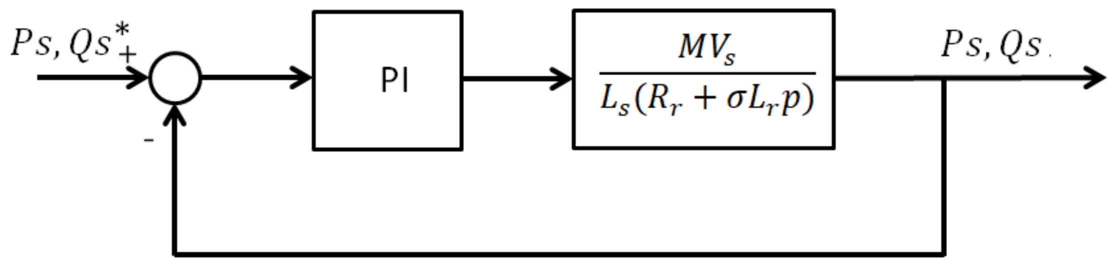

Figure 4.5 Power regulation diagram: Ps and Qs

The open-loop transfer function (OLTF) of Figure 4.5 will be:

$$OLTF(p) = \frac{K_i}{p}\left(p\frac{K_p}{K_i} + 1\right)\frac{\frac{MV_s}{L_s}}{R_r\left(1+p\frac{\sigma L_r}{R_r}\right)} \tag{4.21}$$

For the determination of the gains of power regulators the same approach is opted for as for the currents.

$$K_p = \frac{1}{\tau}\frac{\sigma L_r L_s}{MV_s}$$

$$K_i = \frac{1}{\tau}\frac{R_r L_s}{MV_s} \tag{4.22}$$

τ is the time response for power control system. Simulink model of PI controller is illustrated in Figure 4.6.

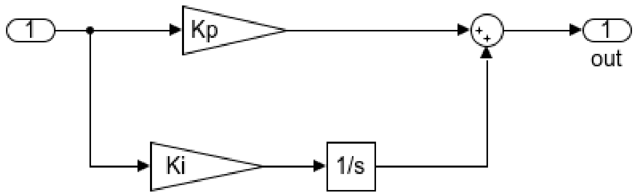

Figure 4.6 Simulink model of PI controller

The proposed Matlab/Simulink model for controlling active and reactive power is shown in the Figure 4.7 below. For this control, four PI controllers are used. The reactive and active powers are controlled by two PI controllers, whereas the rotor currents Ird and Irq are controlled by two PI controllers. The Qc, sigma, Gp, M, Ls and Vs parameters are calculated in the file shown in the Appendix 1.

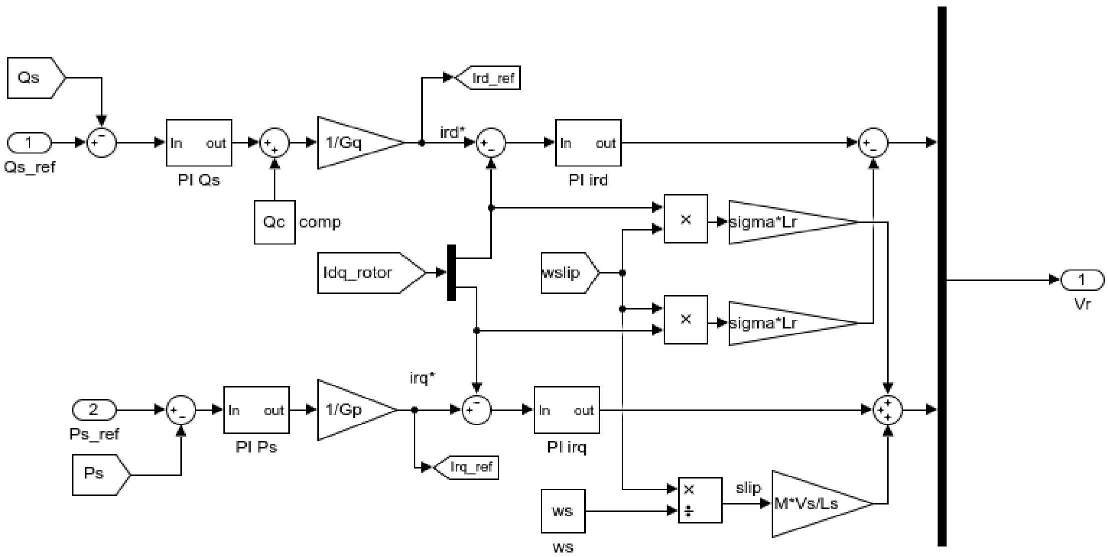

Figure 4.7 Real and reactive power control of DFIG with PI controllers

4.4 Fuzzy Controller

For classical control theory, the PID controller is a standard control structure. However, due to non - linearity in the process plant, performance is severely affected and efficiency is reduced (Hamane *et al.* 2015). The fuzzy control is an intelligent control method for complex systems that uses fuzzy sets, fuzzy linguistic variables, and fuzzy logic inference knowledge to analogize human ways of fuzzy thinking (Ahmadian

2001). Fuzzy control has the advantages of better performance, robustness, and so on without requiring knowledge of the object's mathematical model (Abate and Dosio 1990).

Zadeh introduces the concepts of fuzzy set and fuzzy control in an attempt to control systems that are structurally challenging to model. Since the initial fuzzy control application by Mamdani, fuzzy control has been one of the most active and fruitful research fields in fuzzy set theory, with various industrial applications (Aissaoui and Tahour 2012). Fuzzy logic controllers are progressively being used in various systems with non-linearity and uncertainty (Uzunsoy 2018).

The structure of a fuzzy logic system can be categorized depending on its intended use. The error feedback fuzzy controller, also known as a conventional fuzzy logic controller, is one of the most used types (Ilyas, Jahan and Ayyub 2013).

4.4.1 Principle of fuzzy logic

The implementation of fuzzy logic technique to a real application requires some main steps (Bai and Wang 2006) which are:

- Fuzzification: Fuzzification refers to the process of converting the crisp values of a controller's input variables to fuzzy sets.
- İnference engine: Fuzzy inference is the process that interprets the values of the fuzzy sets in the input and assigns values to the output based on some sets of rules. Mamdani-type and Sugeno-type fuzzy inference systems are the two main types of fuzzy inference systems that can be deployed.
- Defuzzification: The defuzzification process converts fuzzy sets into crisp values. In the literature, there are many defuzzifier methods. One of the most popular easy methods for defuzzification is the centre of gravity (COG).

4.4.2 Design of fuzzy logic controller

The steps described above are used to create a fuzzy logic controller. Figure 3.5 depicts the schematic block of a fuzzy logic controller, which is divided into three sections: fuzzification, inference, and defuzzification.

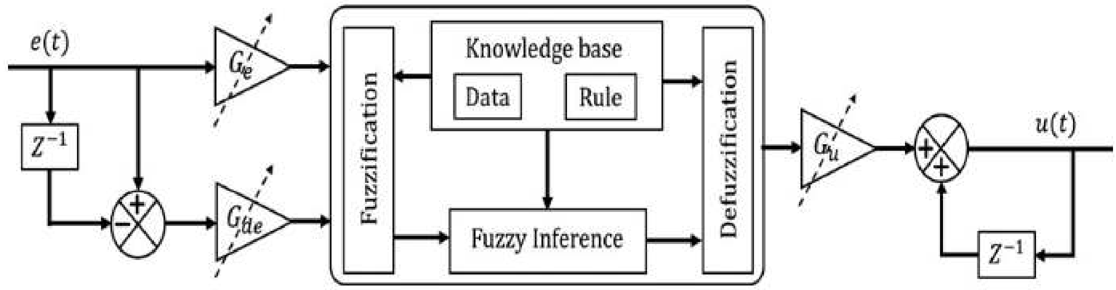

Figure 4.8 Fuzzy logic controller schematic block

In this thesis, four FLC regulators are designed for control of reactive and active powers; two for stator powers and two for rotor currents. There are two inputs and one output for each FLC regulator; the inputs are the error and change of error of controlled variables. The constant gain blocks are implemented as scaling factors Ge, Gde, and Gu to obtain normalized inputs and outputs between -1 and 1 for the fuzzy controller, as shown in Figure 4.8. Selecting these gains is one of the most difficult aspects of the fuzzy logic controller, and if it is done incorrectly, we may not get the best results or possibly have instability.

After identifying the variables to control, the following step is to choose an appropriate membership function for the inputs and outputs. The triangular membership functions, as shown in Figure 4.9, are used in this study since it is a linear function with respect to high performance.

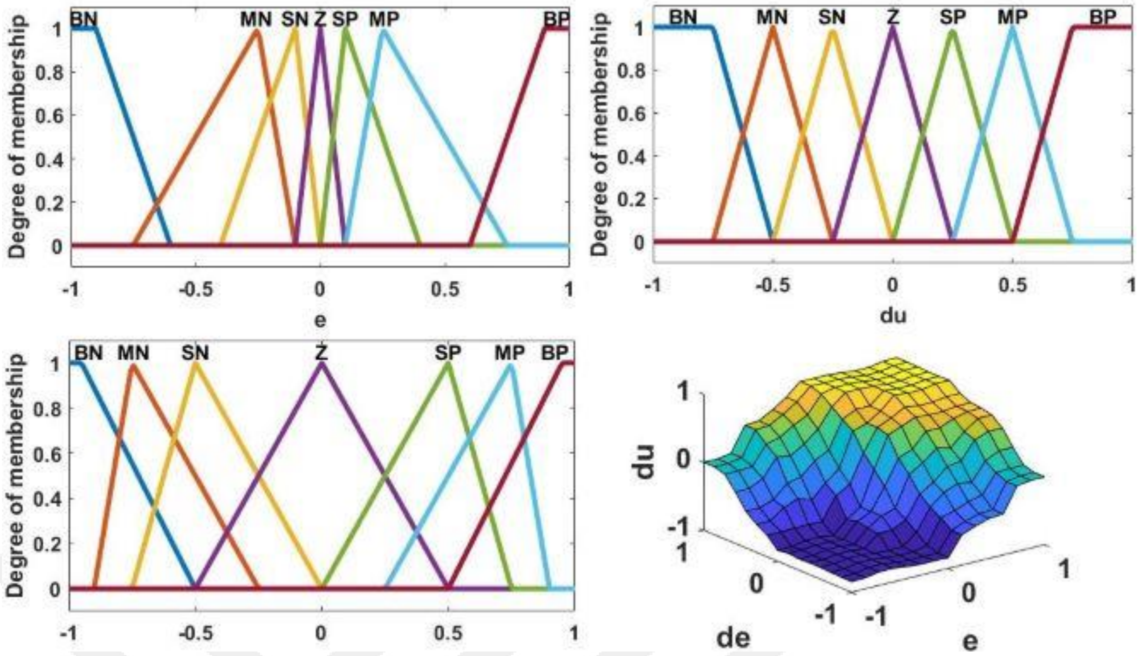

Figure 4.9 Fuzzy logic controller's membership functions parameters and output 3D surface

The quantity of membership functions can be any size, although in fuzzy logic controllers, five to nine fuzzy sets are typically used (Zamzoum *et al.* 2018). Seven sets of fuzzy membership functions were employed for the inputs and the output of all regulators in this study. These fuzzy sets have been defined as: Negative Big (NB), Negative Medium (NM), Negative Small (NS), Zero (Z), Positive Small (PS), Positive Medium (PM), Positive Big (PB). The widths of membership functions triangles and the peak position of membership functions triangles are chosen to improve settling time and accuracy.

The inference system is the second step of the FLC regulator. As the inference strategy, Mamdani's method is applied. The rule bases in this system are more intuitive and simple to understand. It generates basic decision rules using the "IF...THEN" rules and connectors "OR" or "AND". Table 4.1 illustrates the 49 rules derived from seven membership functions for error and seven for error change using Mamdani-type fuzzy inference system.

Table 4.1 Rules table for inference system of fuzzy logic controller

e \ de	NB	NM	NS	Z	PS	PM	PB
NB	NB	NB	NB	NB	NM	NS	Z
NM	NB	NB	NB	NM	NS	Z	PS
NS	NB	NB	NM	NS	Z	PS	PM
Z	NB	NM	NS	Z	PS	PM	PB
PS	NM	NS	Z	PS	PM	PB	PB
PM	NS	Z	PS	PM	PB	PB	PB
PB	Z	PS	PM	PB	PB	PB	PB

Before being used to control the system, the fuzzy set that represents the controller output in linguistic labels must be transformed into a crisp solution variable. A defuzzifier is used to accomplish this. This is done with the help of a defuzzifier. There are many defuzzification alternative methods. The most commonly used techniques are Mean of Maxima (MOM) and Center of Area (COA). The COA approach is used in the majority of control applications (Hilloowala and Sharaf 1996). Also known as the centroid method, this method returns the crisp value that corresponds to the center of the fuzzy set's area (Wang 2001). The centre of gravity method was chosen for defuzzification in this thesis.

Figure 4.10 depicts the proposed Matlab/Simulink model. Rotor currents and stator powers were both controlled by the same FLC design.

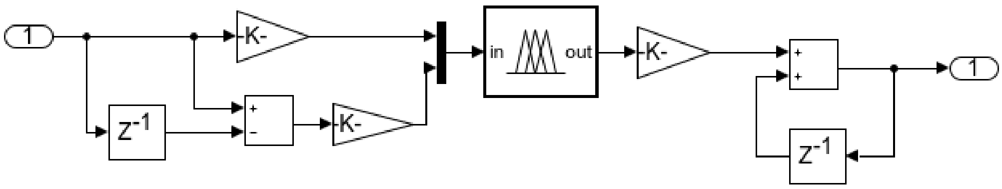

Figure 4.10 Matlab/Simulink model of fuzzy logic controllers

5. SIMULATION RESULTS AND DISCUSSIONS

5.1 Implementation of the System in Matlab/Simulink

To simulate and test the machine model and the performance of the proposed controllers, the MATLAB/Simulink environment was used as simulation tools. Figure 4.1 shows the complete Simulink model. The doubly fed induction generator model is simulated following a transformation from the AC three-phase frame to the dq frame, which simplifies the calculations.

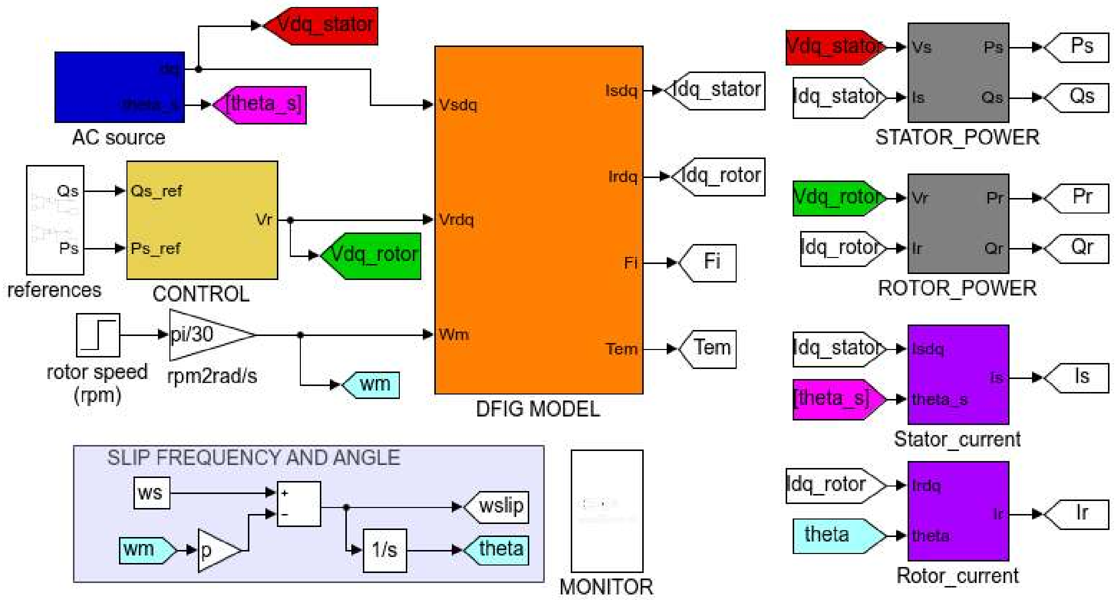

Figure 5.1 Simulink model of the overall system; DFIG and its control.

The Simulink model, as shown in Figure 4.1, consists of seven blocks:

- The stator voltage (in blue)

- The DFIG model (in orange)

- The control (in yellow)

- The calculation of stator and rotor output power (in grey)

- The stator and rotor current transformations from dq to abc (in purple)

The generator stator is directly connected to an alternating voltage source. The blue block in Figure 5.1 represents the source to which the generator stator is connected. Figure 5.2 depicts the content of this block. It consists of a three-phase source, the Clarke transformation, stator variable transformation angle calculation, and park transformation. The Park transformation angle is calculated assuming that the stator flux is properly oriented and that the direct-axis stator voltage Vsd is zero.

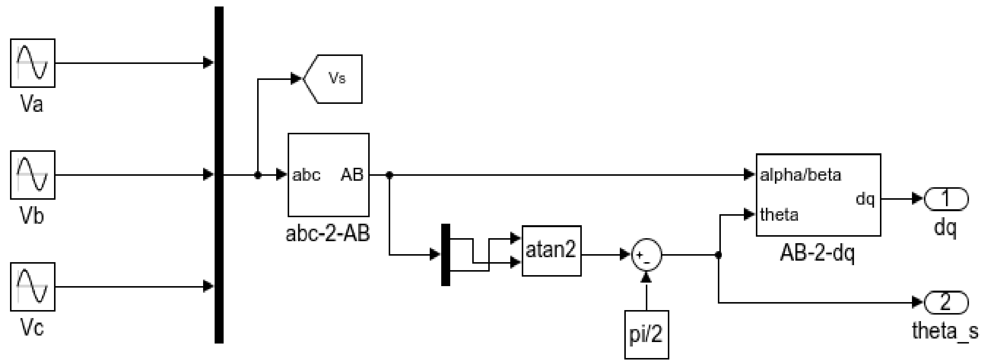

Figure 5.2 Stator voltage transformation block; from abc to dq synchronous frame.

The Simulink block of the DFIG model is composed of two subsystems, which are the generator model presented in Figure 3.10 and the electromagnetic torque calculation illustrated in Figure 3.9. The yellow block is for machine control. Its content is shown in Figure 4.7. The stator and rotor current transformations from dq to abc frame are represented by the two subsystems in purple.

5.2 Simulation Results

A 1.5MW double fed induction machine with the parameters listed in (Table 5.1) is simulated in MATLAB/SIMULINK. The performance of the DFIG system is evaluated under different conditions. First the stator power references are fixed, and the impact of changing the rotor speed on machine performance is examined. The generator's performances with varying references of the powers are then studied while the rotor's speed remains constant.

Table 5.1 DFIG parameters

PARAMETER	VALUE
Stator Power	1,5 MW
Stator Frequency	50 Hz
Nominal Rotor Speed	900-1800 rpm
Number of Pole Pairs	2
Stator Resistance	0,012 Ω
Rotor Resistance	0,021 Ω
Stator inductance	0,0137 H
Stator inductance	0,0136 H
Magnetising inductance	0,0136 H

The generator stator is connected to an AC source of constant frequency and amplitude. The voltage signal to which the stator is connected is shown in Figure 5.3.

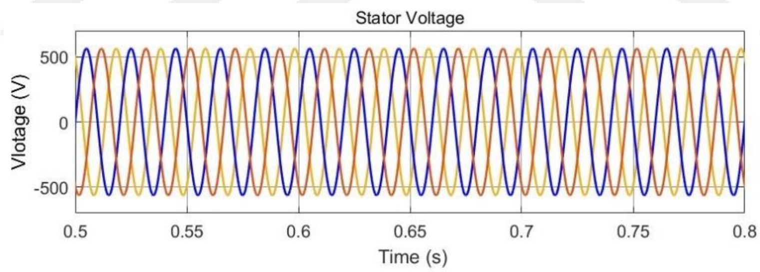

Figure 5.3 Stator Voltage in abc frame (zoom view)

This three-phase alternating source is transformed into dq by using the Clarke and Park transformations and by orienting the stator flux to the direct axis. The stator voltage in the dq frame is depicted in Figure 5.4, and the stator fluxes can be seen in Figure 5.5.

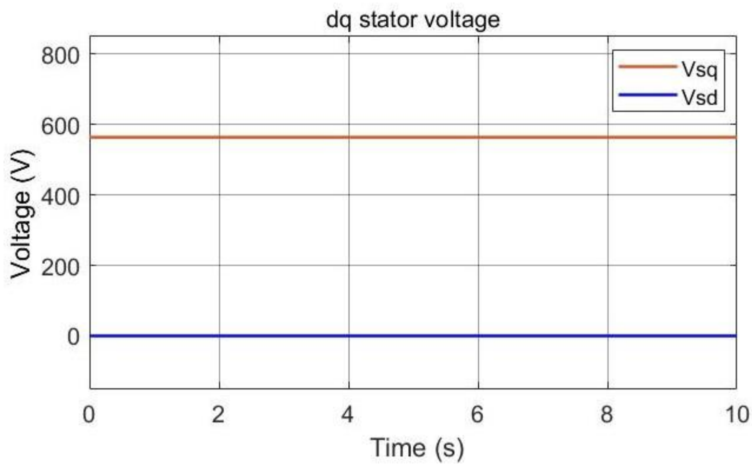

Figure 5.4 Stator Voltage in dq reference frame

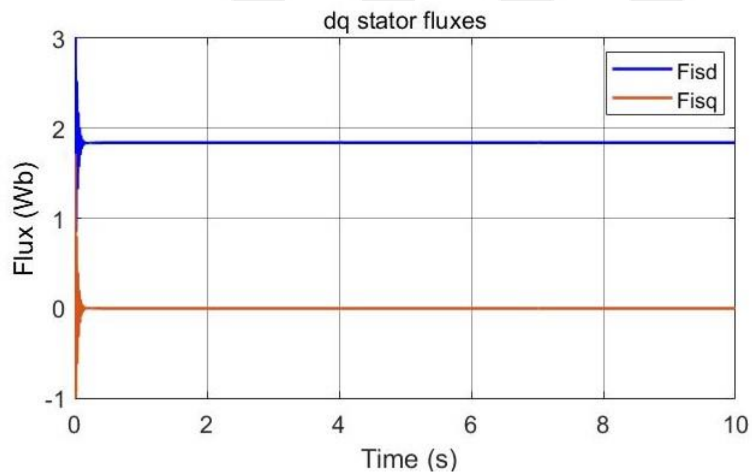

Figure 5.5 Stator fluxes in dq reference frame

In Figure 5.5, the quadrature axis stator flux is zero ($\phi_{sq} = 0$) and the stator flux is equal to the direct axis flux ($\phi_{sd} = \Phi_s$).

5.2.1 Simulation of variable speed operating mode

The purpose of this test is to evaluate the DFIG system with different rotor speeds. The reference active and reactive power profiles are maintained constant in order to examine the performances under the different operating modes of the studied system. By varying the rotor speed, the DFIG system has been tested in sub-synchronous, synchronous, and super-synchronous modes. The active power, reactive power, and rotor speed profiles are listed in (Table 5.2).

Table 5.2 Set points values of the simulated DFIG

TIME (SEC)	ROTOR SPEED (RPM)	OPERATING MODE	PS REFERENCE (MW)	QS REFERENCE (MVAR)
$0 \leq t \leq 4$	1300	Sub-synchronous	-1e6	0
$4<t\leq7$	1500	synchronous	-1e6	0
$7<t\leq10$	1800	Super-synchronous	-1e6	0

PI controller gains used for this simulation are summarised in (Table 5.3).

Table 5.3 PI controllers' gains

GAINS	ROTOR CURRENTS	STATOR POWERS
Proportional Gain	0.003	3
Integral Gain	0.21	12.54

The following graphs display the simulation results carried out by different operation modes.

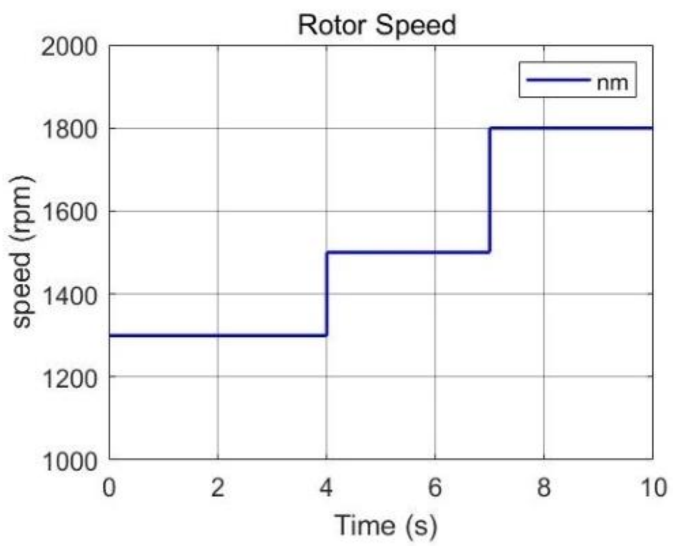

Figure 5.6 Variation of generator speed in rpm

Figure 5.6 depicts the generator's speed profile in revolutions per minute. This speed rises from 1200 rpm to 1500 rpm at 4s. These speeds correspond to the sub-synchronous and synchronous modes, respectively. At 7s, the speed increases to 1800 rpm, and the generator enters super-synchronous mode.

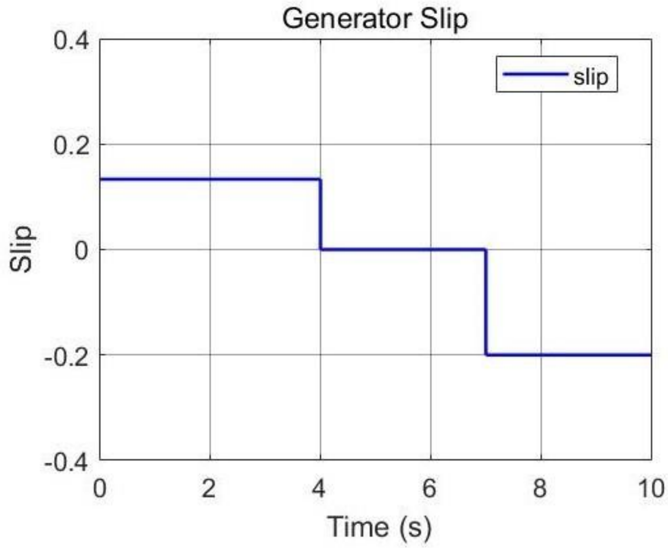

Figure 5.7 Generator slip variation

The generator slip, shown in Figure 5.7, is positive when the generator is operating in sub-synchronous mode. In synchronous mode, it is zero, and in super-synchronous mode, it becomes negative.

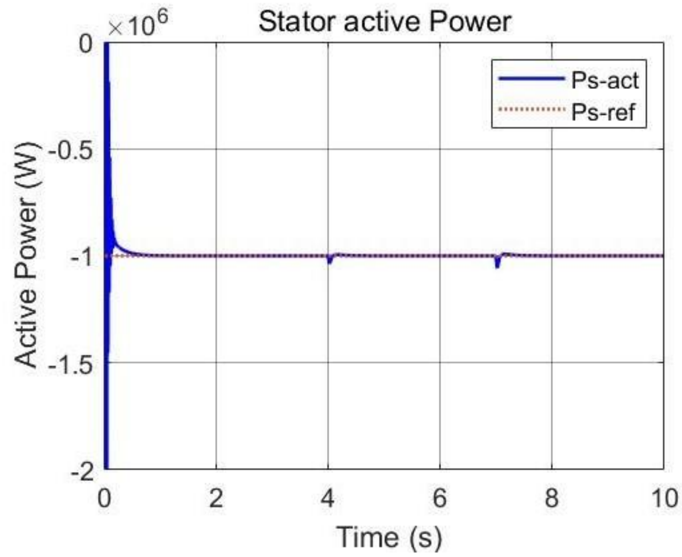

Figure 5.8 Stator active power

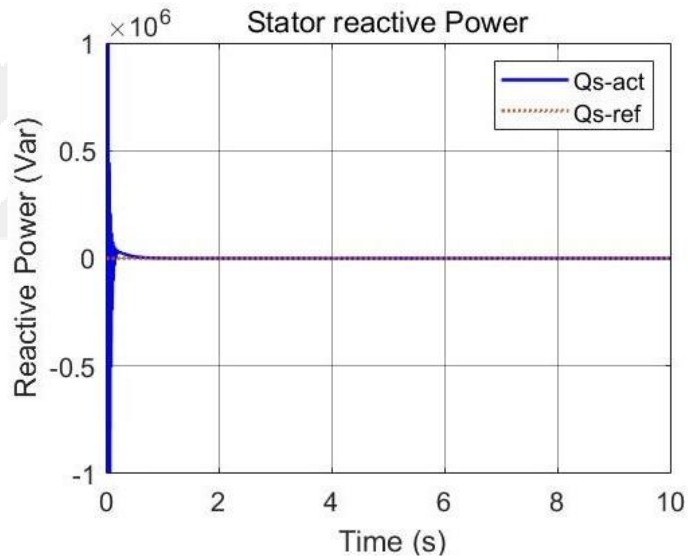

Figure 5.9 Stator reactive power

Figure 5.8 and Figure 5.9 depict the stator's active and reactive power, respectively. During this simulation, their values are held constant. The active power reference was kept at 1MW and the reactive power reference at 0 Var to maintain a unity power factor at the stator.

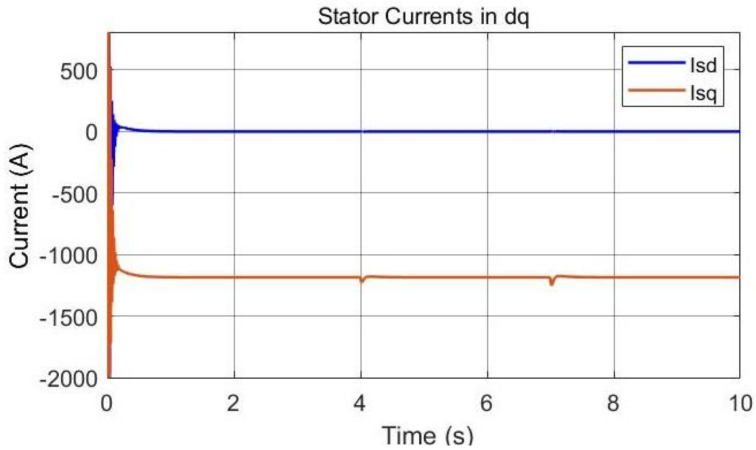

Figure 5.10 d-axis and q-axis of stator currents.

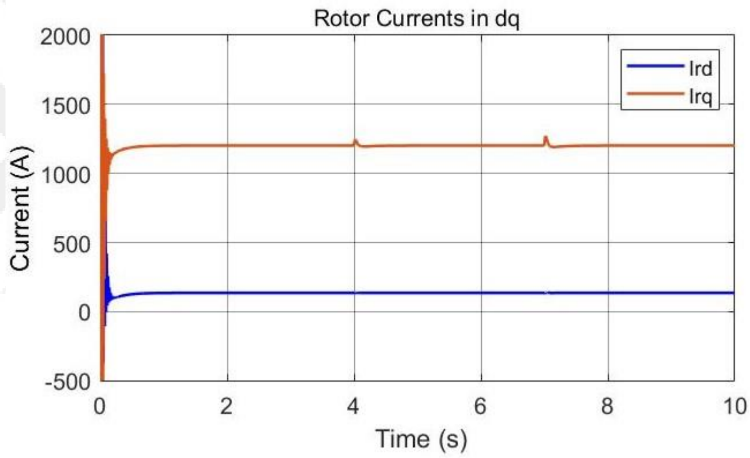

Figure 5.11 d-axis and q-axis of rotor currents.

The stator and rotor current profiles are depicted in Figure 5.10 and Figure 5.11, respectively. These currents are constant in order to maintain the stator powers constant even when the rotor speed changes.

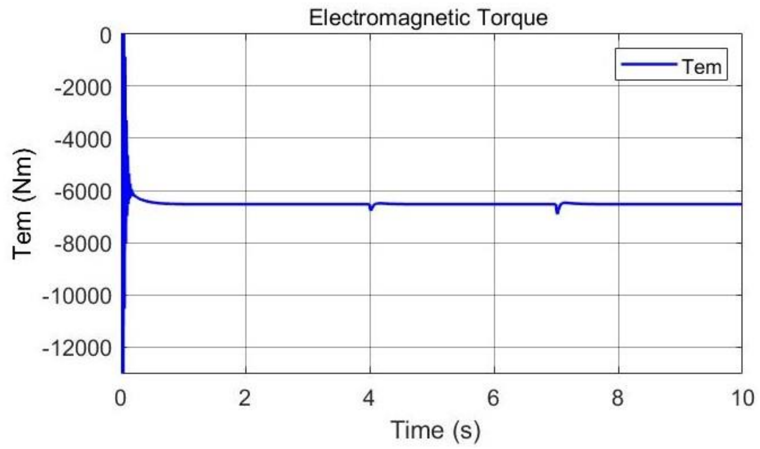

Figure 5.12 Electromagnetic torque profile

Figure 5.12 depicts the electromagnetic torque produced by the generator. The torque is affected by the stator power reference.

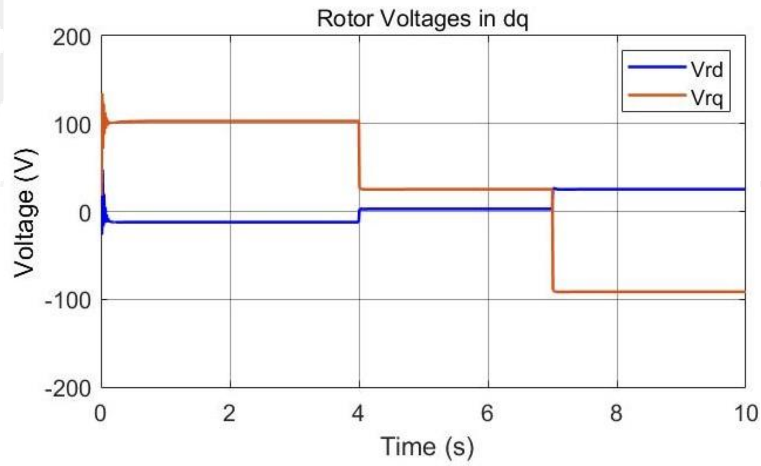

Figure 5.13 d-axis and q-axis of rotor voltages

Figure 5.13 depicts the d and q axes of the rotor voltages. Voltages are not constant and change with rotor speed.

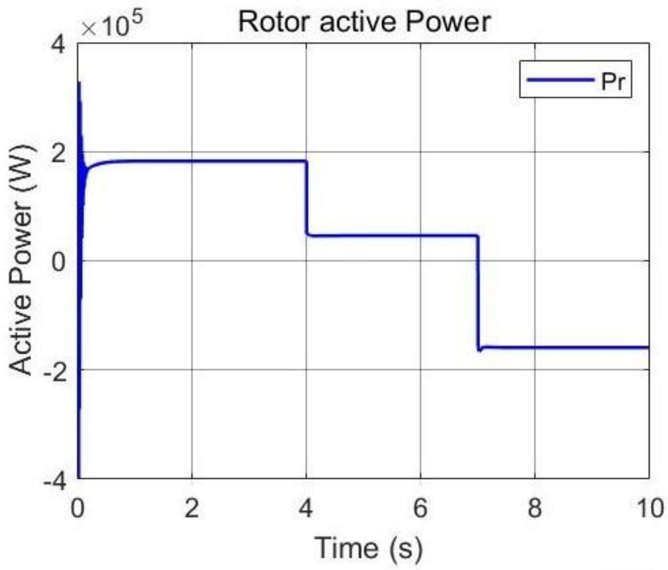

Figure 5.14 Rotor active power

The active power of the rotor is depicted in Figure 5.14. This power varies with generator speed. When the machine is running at sub synchronous speed, the rotor active power is positive, indicating that the generator rotor circuit is consuming active power. At synchronous speed, the generator consumes very little active power. At super synchronous speed, the rotor produces active power.

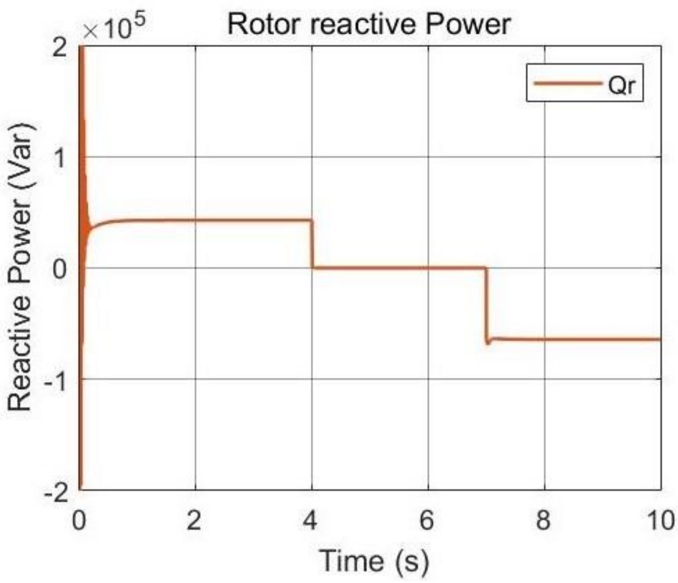

Figure 5.15 Rotor reactive power

Figure 5.14 shows that the generator rotor produces a positive reactive power in sub-synchronous mode, a zero reactive power in synchronous mode, and a negative reactive power in super-synchronous mode.

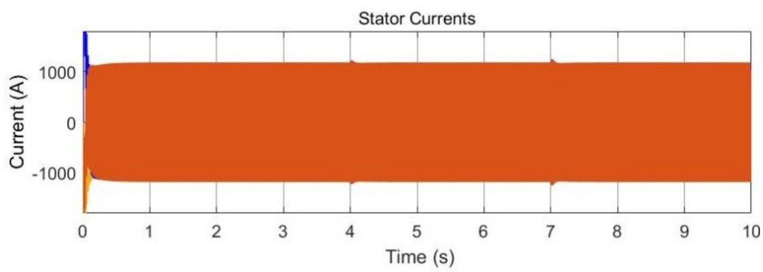

Figure 5.16 Three phase stator currents

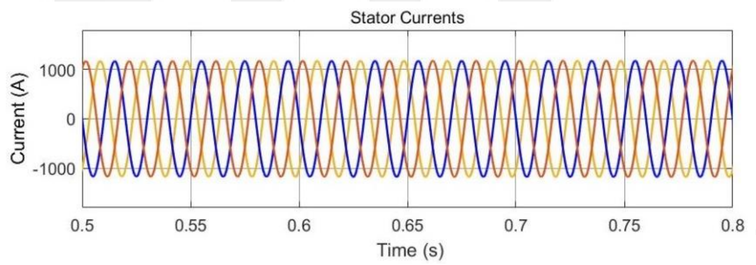

Figure 5.17 Three phase stator currents (zoom view)

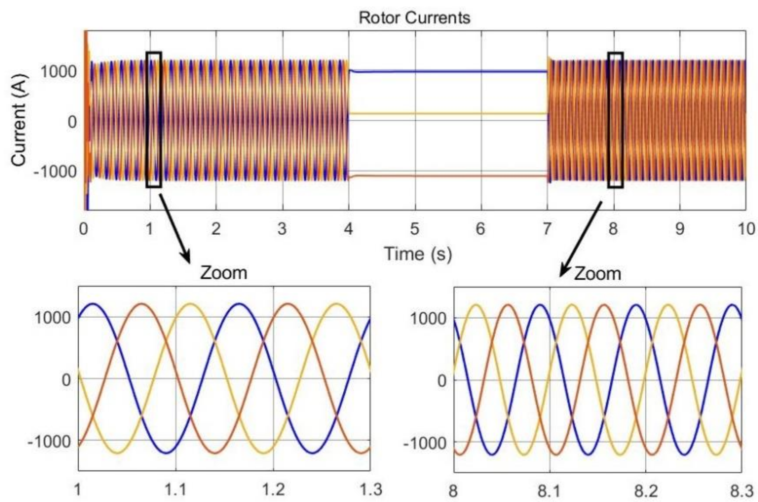

Figure 5.18 Three phase rotor currents

Figure 5.16 depicts the three-phase stator current, while Figure 5.17 zooms in on this stator current. Since the stator is connected to a three-phase source with a fixed frequency, the frequency of the stator current remains constant. The rotor current curve is illustrated in Figure 5.18. For constant stator power references, the rotor current amplitude is constant. The generator's speed affects the frequency of the rotor currents. For a speed that is getting close to synchronous speed, the frequency becomes zero.

5.2.2 Power control with pi and fuzzy logic controller

A PI controller has been used to simulate the DFIG system in order to evaluate the effectiveness of the proposed control. The generator is assumed to operate at a constant speed of 1650 rpm. The generator works in super-synchronous mode since its speed is greater than the synchronous speed. The stator power references are changed as follows:

- At the start of the simulation, the stator's real power reference is 0.8MW. The reference goes from 0.9MW to 1MW at time t=4s and down to 0.9MW at time t=7s.
- At t=0 s, the reactive power reference is 0 Var. This reference changes to 0.1MVar at time t=5s.

Figure 5.19 to Figure 5.24 depict the waveforms of the obtained stator powers, stator currents, rotor currents, and electromagnetic torque.

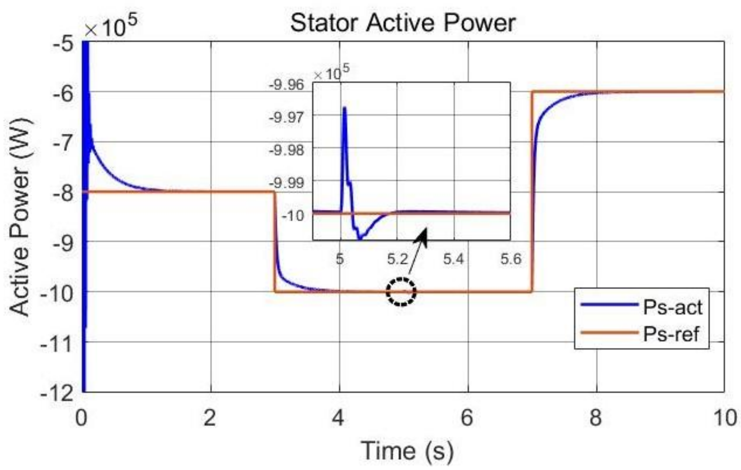

Figure 5.19 Stator active power

The reference and actual stator active power obtained using PI regulators are shown in Figure 5.19. We can see that the active power correctly tracks the value of the reference. PI correctors give better performance by cancelling the static error and have small overshoot. The reference is quickly reached by the active power. At 5s, a disturbance is seen in stator active power. At 5s, a disturbance is seen. The alteration in stator reactive power is to blame for this.

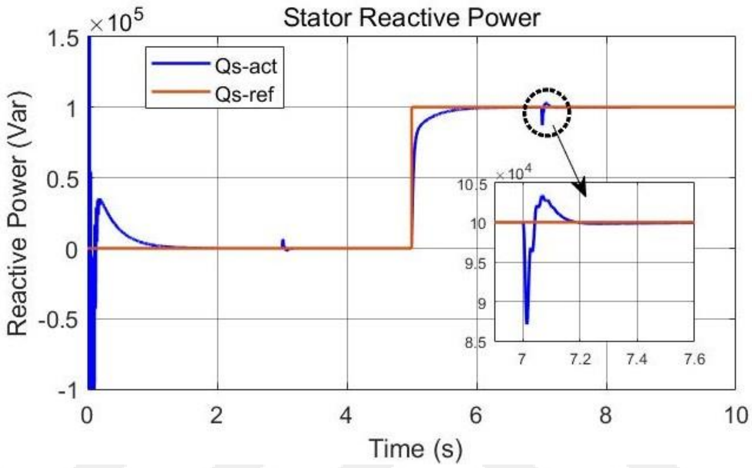

Figure 5.20 Stator reactive power

Figure 5.20 depicts the stator's reactive power. The set point for reactive power is quickly reached for active power. At t=4s and t=7s, there are disturbances in the reactive power waveform. To view the disturbance amplitude clearly, a zoom was applied at t =7 s.

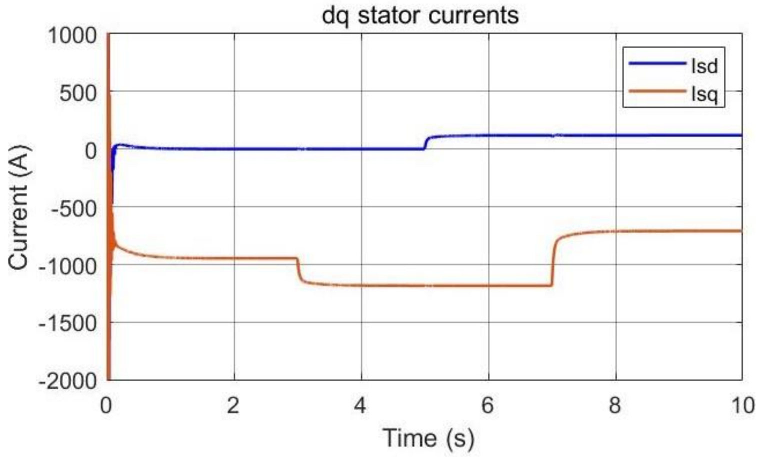

Figure 5.21 Stator currents

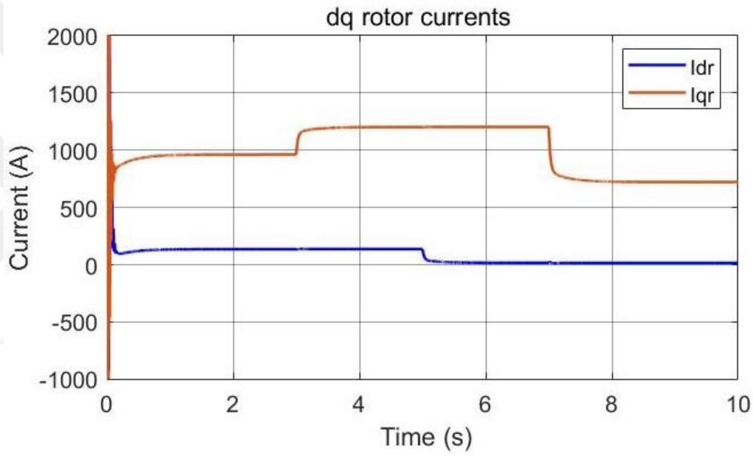

Figure 5.22 Rotor currents

Figure 2.21 shows the waveforms of the stator current, whereas Figure 2.22 illustrates the waveforms of the rotor current. It is evident that currents change when the power references change. Both the direct and quadrature axes of the stator and rotor currents vary with the reactive power and the active power, respectively. The rotor current q-axis decreases and the stator current q-axis increases as the active power rises. Additionally, as the reactive power is increased, the d-axis of the stator current rises while that of the rotor current decreases. As a result, it can be shown that active and reactive powers are properly decoupled.

Results from the proposed control with PI regulators are acceptable. In accordance with their respective references, active and reactive powers are independently regulated.

Small disturbances are observed on the waveforms of active power, reactive power, and electromagnetic torque at the moment of change of reference of active and reactive powers.

To increase the proposed control performance, the PI regulators are replaced by fuzzy logic regulators. Table 5.4 lists the scaling factors for fuzzy logic controllers. Figure 5.23 depicts the proposed control with fuzzy regulators.

Table 5.4 Scaling factors of fuzzy logic controllers

SCALING FACTORS	ROTOR CURRENTS	STATOR POWERS
Ge	6.33e-4	1e-7
Gde	3e-5	5e-9
Gu	2	1.2e5

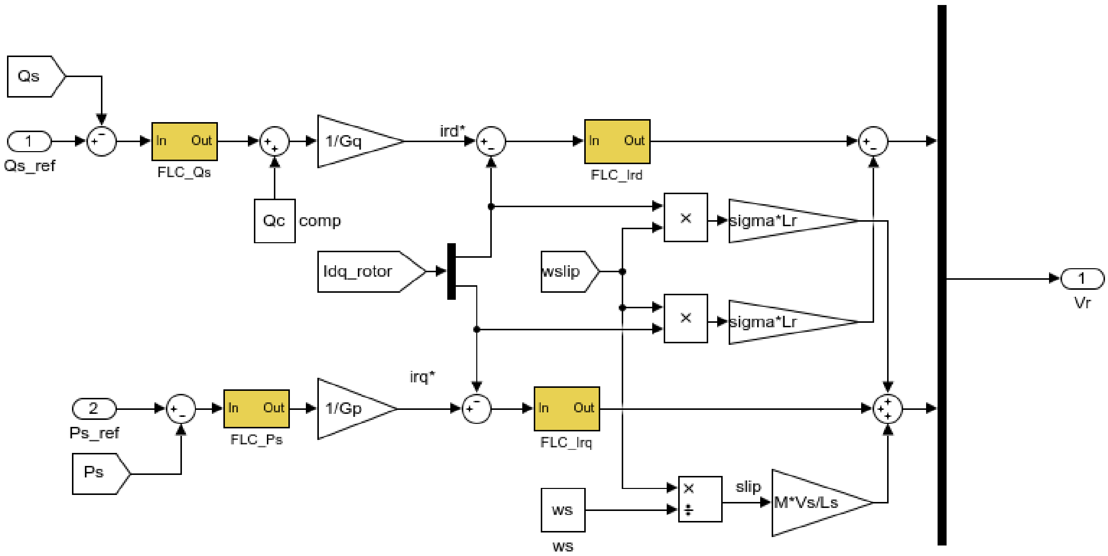

Figure 5.23 The control block with fuzzy logic controllers

Figures 5.24 to 5.27 show the results obtained with the fuzzy logic regulators.

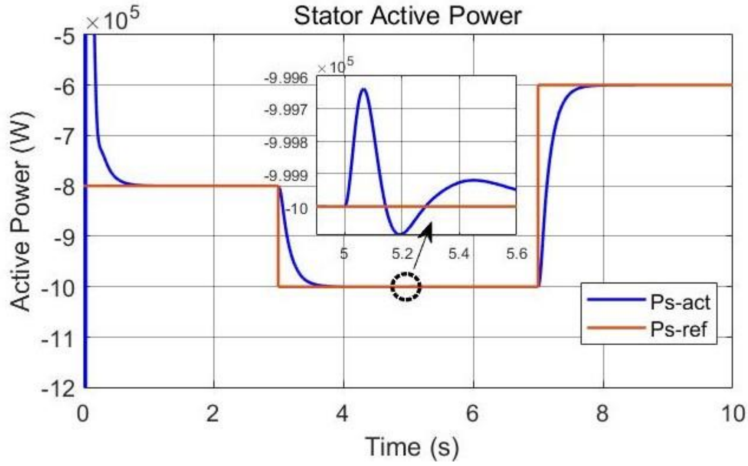

Figure 5.24 Stator active power

Figure 2.24 shows that the control with fuzzy logic provides good results. The active power response is fast and stable, with small overshoot and zero static error. The disturbance caused by reactive power change on active power was reduced by fuzzy logic.

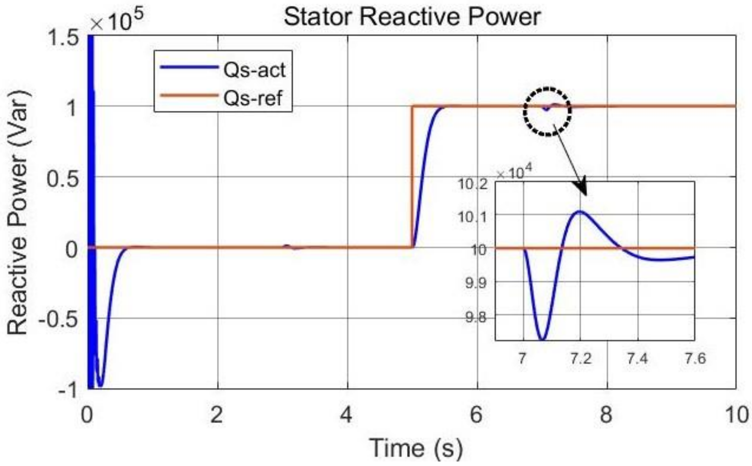

Figure 5.25 Stator reactive power

Figure 5.25 depicts the stator's reactive power response. The reference is set to 0Var at the beginning of the simulation in order to have a stator power factor of unity. To evaluate the effectiveness of the control technique, the reference changes to 0.1MVar at time t=5s. With negligible overshoot, the reactive power properly tracks the reference. With this control, the disturbance amplitude is minimal.

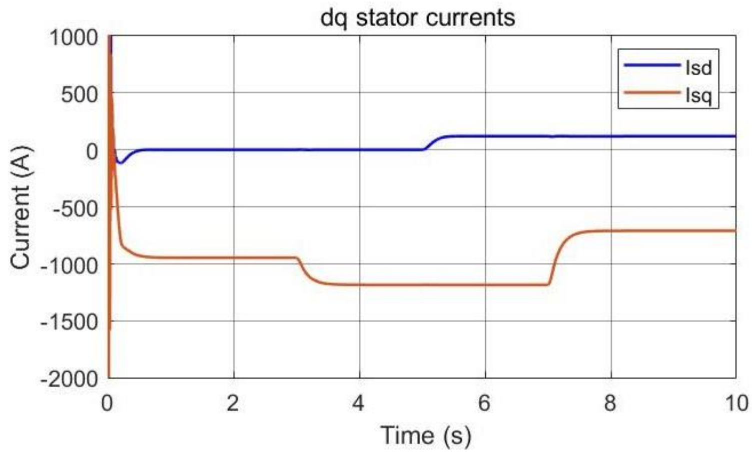

Figure 5.26 Stator currents

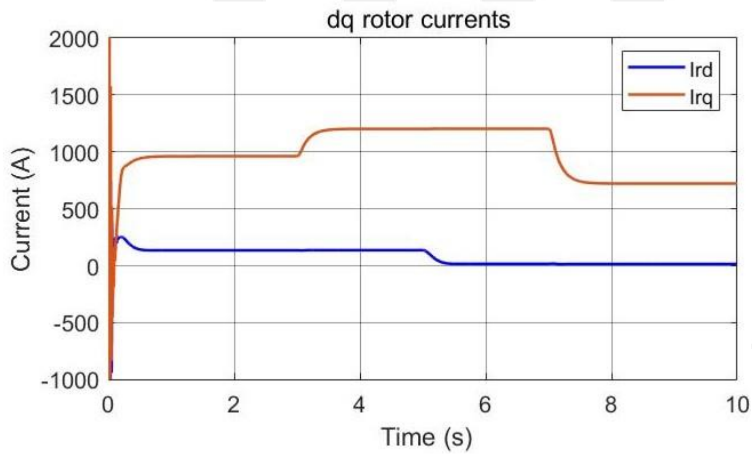

Figure 5.27 Rotor currents

Figure 5.26 and Figure 5.27 of stator and rotor currents show that active and reactive powers are decoupled. The components of the current d-axis vary with reactive power and the current q-axis with active power.

To compare the control techniques employing PI controllers and fuzzy logic controllers, the waveforms are plotted on same graphs. Figure 5.29 to Figure 5.32 show the results obtained with the control strategies.

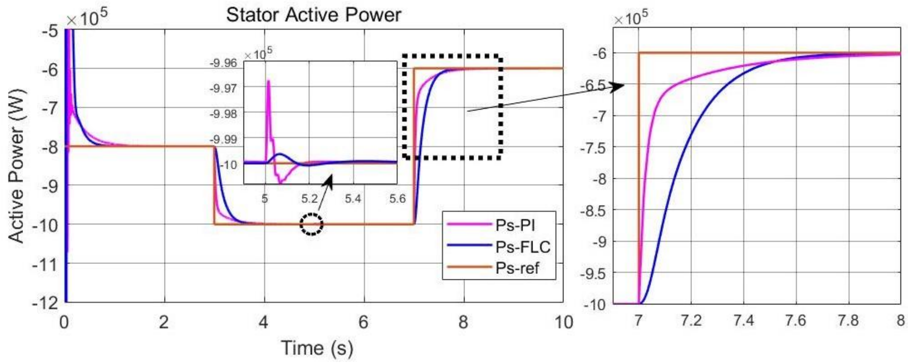

Figure 5.28 Stator active power obtained with PI and fuzzy logic controller

The comparative study of the active power response is shown in Figure 5.28. The performance comparison of the two controllers is tabulated in (Table 5.5).

Table 5.5 Performance comparison between controllers for active power

CONTROLLERS	OVERSHOOT (%)	RİSE TİME 90% (s)	SETTLİNG TİME (s)
PI	0.3	0.2	1.4
Fuzzy logic	0.1	0.37	1

Both controllers give almost the same active power profile. PI controllers have a better rise time than FLC controllers. The settling time is better for fuzzy logic controllers and the static errors in both controllers are zero. The effect of disturbance is very small in the fuzzy logic controller strategy, as can be seen in Figure 5.28.

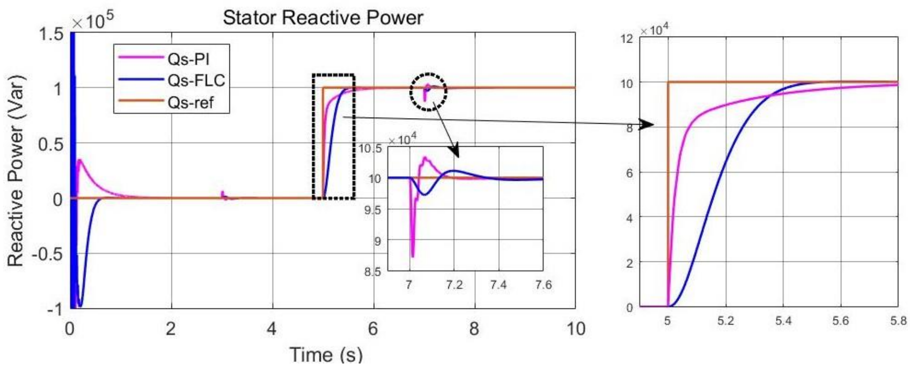

Figure 5.29 Stator reactive power obtained with PI and Fuzzy logic controller

As can be seen in Figure 5.29, PI controllers and fuzzy logic controllers give improved results for reactive power control of the generator stator. The performance comparison of the two controllers is tabulated in (Table 5.6).

Table 5.6 Performance comparison between controllers for reactive power

CONTROLLERS	OVERSHOOT (%)	RİSE TİME 90% (s)	SETTLİNG TİME (s)
PI	12.5	0.21	1.4
Fuzzy logic	6	0.33	0.5

The reactive power quickly reaches the reference value for the two controllers. The rise time is preferable for PI controllers. However, fuzzy logic controllers improve disturbance rejection, small overshoot and better settling time.

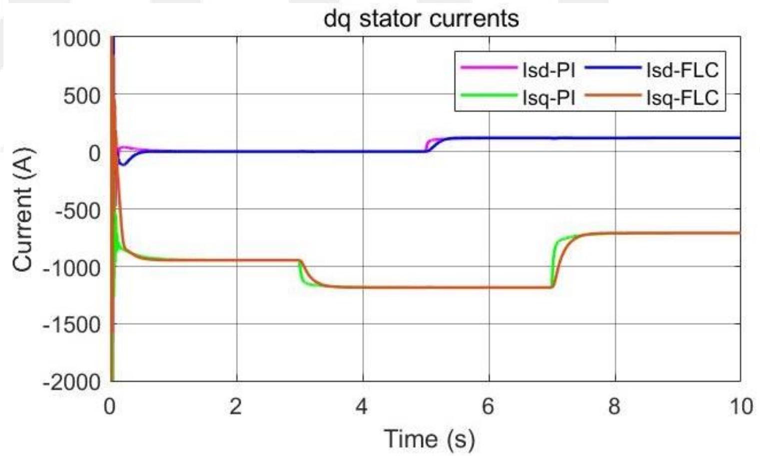

Figure 5.30 Stator currents with PI and FLC

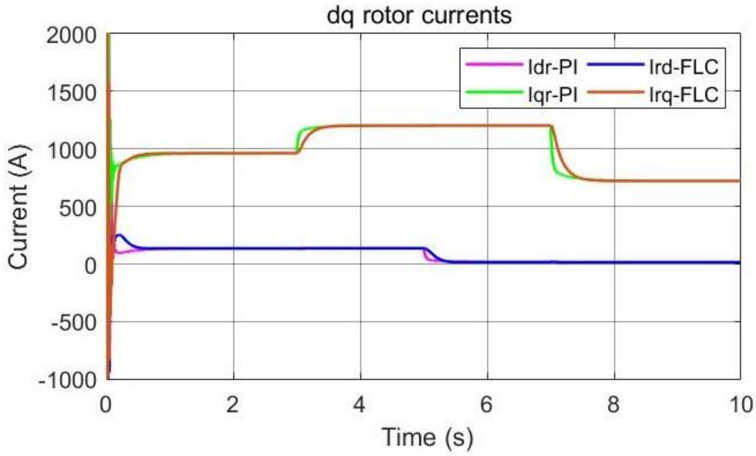

Figure 5.31 Rotor currents with PI and FLC

The dq current of the stator and rotor are shown in Figure 5.30 and Figure 5.31, respectively. Variation in reactive power cause changes in the magnitudes of current Isd and Ird. Thus the magnitudes of the current Isq and Irq are influenced by the active power. This demonstrates that a satisfactory decoupling between active and reactive power is achieved using the two control schemes.

According to the results of the simulations performed, the proposed control technique gives a good decoupled control of the active and reactive power. By suppressing steady state error for power controls, PI and fuzzy logic controllers both provide optimal performance. Fuzzy logic regulators, which improve system stability by reducing the perturbations seen during power changes, have a slower response time than PI regulators.

6. CONCLUSION AND RECOMMENDATIONS

In this thesis, control of a doubly-fed induction generator system has been considered. More specifically, the rotor side converter's control of the stator's active and reactive power is investigated. The model of a double-fed induction generator has been developed in the dq reference frame rotating at synchronous speed by applying Clarke and Park transformations.

The stator powers were controlled by regulating the rotor currents using a field-oriented control-based scheme. A decoupled control of active and reactive power is carried out by using PI controllers and fuzzy logic controllers. The synthesis of a proportional-integral (PI) controller and a fuzzy logic controller (FLC) is performed.

Using the specifications of a 1.5MW dual-fed induction generator, the dynamic model of the proposed entire system was created in Matlab/Simulink. To verify the performance of the proposed scheme, a computer simulation was conducted.

The performance of PI and fuzzy logic controllers has been presented and they have been compared between them. The effectiveness of the controllers is evaluated. The main conclusions that can be deduced from the simulation results are summarized below:

- The performance of the proposed schemes is presented for different active and reactive power references. The PI and FLC controllers gave fast and good responses.

- Both techniques achieve a good decoupling of active and reactive power. They have the ability to control the stator powers independently.

- To reference variations, the technique utilising PI controllers has a faster response time than fuzzy logic controllers. And the fuzzy logic controllers have better overshoot and settling time.

- The comparison analysis showed that the fuzzy logic controllers' performance was slightly superior to that of PI controllers when handling disturbances.

According to this thesis's study results, the following areas need further investigation:

- The performance of PI and fuzzy logic controllers can be increased by implementing optimization techniques like the genetic algorithm.

- Application of additional, more complex controllers, such as sliding mode and adaptive fuzzy PI controllers.

- Due to the benefits of not requiring coordinate transformations and rotor current control loops, direct power control can be taken into consideration.

REFERENCES

Abad, G. and Iwanski, G. 2014. Properties and control of doubly fed induction machine, Power electronics for renewable energy systems, transportation and industrial *applications*. Abu-Rub, H., Malinowski, M. and Al-Haddad, M., IEEE PRESS. *pp:* 270-318. UK

Abate, M. and Dosio, N. 1990. Use of fuzzy logic for engine idle speed control. SAE Transactions, 99: 873-880.

Adamowicz, M. and Strzelecki, R. 2008. Cascaded doubly fed induction generator for mini and micro power plants connected to grid. *13th International Power Electronics and Motion Control Conference*, pp. 1729-1733.

Ahmadian, M. 2001. Active control of vehicle vibratıon. *Encyclopedia of Vibration*. doi:10.1006/rwvb.2001.0193.

Aissaoui, A. G., and Tahour, A. 2012. Application of Fuzzy Logic in Control of Electrical Machines, Fuzzy Logic - Controls, Concepts, Theories and Application, Dadios, E.P, InTech, pp: 107-129, Croatia

Akter, M. P., Mekhilef, S., Tan, N. M. L., and Akagi, H. 2015. Model predictive control of bidirectional AC-DC converter for energy storage system. Journal of Electrical Engineering and Technology, 10(1), 165-175.

Amorim, A. E., Oliveira, F. D., and Simonetti, D. S. 2021. A new hybrid multilevel back-to-back converter for doubly fed induction generator-based wind turbines' fault supportability. International Transactions on Electrical Energy Systems, 31(3), e12793.

Bai, Y., and Wang, D. 2006. Fundamentals of fuzzy logic control-fuzzy sets, fuzzy rules and defuzzifications, Advanced fuzzy logic technologies in industrial applications. Springer , pp. 17-36 , London.

Bakır, H.,Merabet, A. and Kulaksız, A. A. 2020. Power control in the dfig-based wind energy system using opal-rt. European Journal of Science and Technology, 373-379.

Bayhan, S., Abu-Rub, H., and Ellabban, O. 2016. Sensorless model predictive control scheme of wind-driven doubly fed induction generator in dc microgrid. IET Renewable Power Generation, 10(4), 514-521.

Behara, R. K., and Behara, K. 2022. Simulation Analysis of DFIG Integrated Wind Turbine Control System, Wind Turbines - Advances and Challenges in Design, Manufacture and Operation, Maalawi, K.Y. IntechOpen,

Bekakra, Y. 2010. Etude et commande du moteur asynchrone à double alimentation (MADA) par différentes techniques avancées. PhD. Thesis, University of Eloued, 106 pages, Alger.

Bharti, O. P., Saket, R. K., and Nagar, S. K. 2018. Controller design of DFIG-based WT by using DE-optimization techniques. In 2018 SICE International Symposium on Control Systems (SICE ISCS) (pp. 128-135). IEEE.

Boubzizi, S., Abid, H. and Chaabane, M. 2018. Comparative study of three types of controllers for dfig in wind energy conversion system. *Protection and Control of Modern Power Systems*, *3*(1), 1-12.

Cho, K. M., Oh, W. S., Kim, Y. T., and Kim, H. J. 2007. A new switching strategy for pulse width modulation (PWM) power converters. IEEE Transactions on Industrial Electronics, 54(1), 330-337.

Chouhan, N. S. 2010. Doubly fed induction generator with integrated energy storage system for smoothening of output power. Msc. Thesis, Missouri University, 108 pages, Missouri.

Çalgan, H. 2016. Çift beslemeli asenkron generatörün pi ve adaptif kayan kip güç kontrolü . MSc. Thesis, Balıkesir University, 71 pages, Balıkesir.

Dahiya, V. and Leena, G. 2019. Simulation and modeling of DFIG wind farm in wind energy conversion system. *Int. J. Appl. Eng. Res*, *14*(12), 2844-2849.

Díaz, G., González-Morán, C., and Viescas, C. 2013. State-space representation of DFIG-based wind power plants. IET Renewable Power Generation, 7(3), 254-264.

Drid, S., Nait-Said, M. S., and Makouf, A. 2006. Regular paper Doubly Fed Induction Generator Modeling and Scalar Controlled for Supplying an Isolated Site. *J. Electrical Systems*, *2*(2), 103-115.

Ehlert, D. and Wrede, H. 2007. Wind turbines with doubly-fed induction generator systems with improved performance due to grid requirements. *IEEE Power Engineering Society General Meeting*.

El Ouanjli, N., Derouich, A., El Ghzizal, A., Chebabhi, A., and Taoussi, M. 2017. A comparative study between FOC and DTC control of the Doubly Fed Induction Motor (DFIM). In *2017 International Conference on Electrical and Information Technologies (ICEIT)* (pp. 1-6). IEEE.

Elghali, S. B., Benbouzid, M. E. H. and Charpentier, J. F. 2010. Modelling and control of a marine current turbine-driven doubly fed induction generator.*IET Renewable Power Generation*, *4*(1), 1-11.

Eltamaly, A. M., Al-Saud, M. S., and Abo-Khalil, A. G. 2020. Dynamic control of a DFIG wind power generation system to mitigate unbalanced grid voltage. IEEE Access, 8, 39091-39103.

Gupta, S., and Wadhwani, S. 2014. Dynamic modeling of induction motor using rotor rotating reference frame. International Journal of Advance Research in Electrical, Electronics and Instrumentation Engineering, 3(6).

Hamane, B., Doumbia, M. L., Bouhamida, M., Draou, A., Chaoui, H., and Benghanem, M. 2015. Comparative study of PI, RST, sliding mode and fuzzy supervisory controllers for DFIG based wind energy conversion system. *International journal of renewable energy research*, *5*(4), 1174-1185.

Hamane, B., Doumbia, M. L., Cheriti, A., and Belmokhtar, K. 2014. Comparative analysis of PI and fuzzy logic controllers for matrix converter. In 2014 Ninth International Conference on Ecological Vehicles and Renewable Energies (EVER) (pp. 1-7). IEEE.

Hassan, A. A., El-Sawy, A. M., and Kamel, O. M. 2013. Direct torque control of a doubly fed induction generator driven by a variable speed wind turbine. *JES. Journal of Engineering Sciences*, *41*(1), 199-216.

Hilloowala, R. M., and Sharaf, A. M. 1996. A rule-based fuzzy logic controller for a PWM inverter in a standalone wind energy conversion scheme. IEEE Transactions on Industry Applications, 32(1), 57-65.

Hlaing, S. 2014. Basic concepts of doubly fed induction generator driven by wind energy conversion system. Int. J. Sci. Eng. Technol. Res, 3(15-2014), 3242-3246.

Hussien, M. G., and Hassan, A. E. W. 2019. Mathematical Analysis of the Small Signal Model for Voltage-Source Inverter in SPMSM Drive Systems. In 2019 21st

International Middle East Power Systems Conference (MEPCON) (pp. 540-549). IEEE.

Ilyas, A., Jahan, S., and Ayyub, M. 2013. Tuning of conventional PID and fuzzy logic controller using different defuzzification techniques. International journal of scientific and technology research, 2(1), 138-142.

Jenkal, H., Bossoufi, B., Boulezhar, A., Lilane, A., and Hariss, S. 2020. Vector control of a Doubly Fed Induction Generator wind turbine. Materials Today: Proceedings, 30, 976-980.

Kainth, H. S., and Sharma, G. 2014. A new method for differential protection in power transformer. Journal of Electrical and Electronics Engineering, 9(2), 64-70.

Kearney, J. 2013. Grid voltage unbalance and the integration of DFIG's. Phd Thesis, School of Electrical and Electronic Engineering Dublin Institute of Technology, 335 pages, Dublin.

Khan, D., Ahmed Ansari, J., Aziz Khan, S., and Abrar, U. 2020. Power optimization control scheme for doubly fed ınduction generator used in wind turbine generators. *Inventions*, *5*(3), 40.

Kılıçaslan, M. F. 2015. Rüzgar türbinlerinde çift beslemeli asenkron jeneratör denetimi. MSc. Thesis, Kırıkkale University, 94 pages, Kırıkkale.

Korkmaz, F., Topaloğlu, İ., Çakir, M. F., and Gürbüz, R. 2013. Comparative performance evaluation of FOC and DTC controlled PMSM drives. In *4th international conference on power engineering, energy and electrical drives* (pp. 705-708). IEEE.

Kumar, A. P., Parimi, A. M., and Rao, K. U. 2015. Investigation of small PMSG based wind turbine for variable wind speed. International Conference on Recent Developments in Control, Automation and Power Engineering (RDCAPE) (pp. 107-112). IEEE.

Kumar, A., and Ramesh, T. 2015. Direct field oriented control of induction motor drive. *Second International Conference on Advances in Computing and Communication Engineering* (pp. 219-223). IEEE.

Kumar, P., and Choudhary, R. 2014. Study of doubly fed induction generator characteristics. *Int J Recent Res Aspects*, *2*(3), 1-6.

Li, W., Xu, Z., and Zhang, Y. 2019. Induction motor control system based on FOC algorithm. In *2019 IEEE 8th Joint International Information Technology and Artificial Intelligence Conference (ITAIC)* (pp. 1544-1548). IEEE.

Mahboub, M. A. 2018. Modélisation et commande d'un système éolien à base d'une génératrice double alimentée sans balais. Msc. Thesis, Ferhat Abbas-Setif University, 144 pages, Algeria

Malik, N. U. R. 2015. Modelling, Analysis, and Control Aspects of a Rotating Power Electronic Brushless Doubly-Fed Induction Generator. PhD Thesis, KTH School of Electrical Engineering and Computer Science, 96 pages, Sweden.

Moulay, F., Habbatti, A. and Hamdaoui, H. 2019. Application and control of a doubly fed induction machine integrated in wind energy system. *Instrumentation Mesure Métrologie*, *18*(3), 257-265.

Moussa, O., Abdessemed, R. and Benaggoune, S. 2019. Super-twisting sliding mode control for brushless doubly fed induction generator based on wecs. *International Journal of System Assurance Engineering and Management*, *10*(5), 1145-1157.

Mwaniki, J., Lin, H. and Dai, Z. 2017. A condensed introduction to the doubly fed induction generator wind energy conversion systems. *Journal of Engineering*.

Ortatepe, Z. 2020. A new model ımplementation for doubly fed ınduction generator used in variable speed wind turbines. Phd Thesis, Ankara Yıldırım Beyazıt University, 169 pages, Ankara.

Ötkün, O. 2020. Scalar speed control of induction motors with difference frequency. *Politeknik Dergisi*.

Petersson, A. 2005. Analysis, modeling and control of doubly-fed induction generators for wind turbines. PhD. Thesis, Chalmers Tekniska Hogskola University, 148 pages, Sweden.

Poitiers, F. 2003. Etude et commande des génératrices asynchrones pour l'utilisation de l'énergie éolienne. PhD Thesis, Nantes University, 203 pages, Nantes.

Pokharel, B. 2011. Modeling, control and analysis of a doubly fed induction generator based wind turbine system with voltage regulation. Msc. Thesis, Tennessee Technological University, 303 pages,.Tennessee.

Popescu, M. 2000. Induction motor modelling for vector control purposes. Report, Helsinki University of Tehnology, 143 pages, Helsinki.

Radaideh, A., Bodoor, M. M., and Al-Quraan, A. 2021. Active and reactive power control for wind turbines based dfıg using lqr controller with optimal gain-scheduling. Journal of Electrical and Computer Engineering.

Rahmani, O., Amiri, P., Mokhtari, Z., and Amirjamshidi, Z. 2015. Simulation and comparison of control methods of doubly fed ınduction generator in energy conversion system. *Ciência e Natura*, *37*, 195-204.

Raju, N., and Raju, P. S. 2015. Modeling and Simulation of AC/DC in Wind Generation Fed Induction Motor Drive. International Journal of Scientific Engineering and Technology Research, 2319-8885.

Resmi, R., Agoram, C. A., Adithya, P., and Vanitha, V. 2015. Design and analysis of brushless doubly fed induction generator. *Procedia Technology*, *21*, 604-610.

Sahri, Y., Tamalouzt, S., and Belaid, S. L. 2018. Direct torque control of DFIG driven by wind turbine system connected to the grid. In *2018 International Conference on Wind Energy and Applications in Algeria (ICWEAA)* (pp. 1-6).

Sarma, N., Tuohy, P.M., Apsley, J.M., Wang, Y. and Djurović, S. 2018. DFIG stator flux-oriented control scheme execution for test facilities utilising commercial converters. IET Renewable Power Generation, 12: 1366-1374. https://doi.org/10.1049/iet-rpg.2018.5195

Sunny, A. C., Das, B., Kasari, P. R., Sarkar, A., Bhattacharya, S., and Chakrabarty, A. 2016. Svpwm based decoupled control of active and reactive power for single stage grid connected solar PV system. In 2016 IEEE 7th Power India International Conference (PIICON) (pp. 1-6). IEEE.

Şahin, M. E. 2020. Comparison of ig and dfig for wind power generation systems. *Gazi Mühendislik Bilimleri Dergisi* , 6 (3) , 230-241.

Tir, Z., Rajeai, H., and Abdessemed, R. 2010. Analysis and vector control of a cascaded doubly fed induction generator in wind energy applications. *Revue des Energies Renouvelables*, 347-358.

Ulu, C. and Kömürgöz, G. 2017. Electrical design and testing of a 500 kw doubly fed induction generator for wind power applications. *Turkish Journal of Electrical Engineering and Computer Sciences*, *25*(2), 1278-1290.

Uzunsoy, E. 2018. A brief review on fuzzy logic used in vehicle dynamics control. Journal of Innovative Science and Engineering, 2(1), 1-7.

Wang, K. 2001. Computational intelligence in agile manufacturing engineering. Agile manufacturing: The 21st Century Competitive Strategy, Gunasekran, A. ELSEVIER SCIENCE, pp. 297–315, UK.

Zamzoum, O., El Mourabit, Y., Errouha, M., Derouich, A. and El Ghzizal, A. 2018. Power control of variable speed wind turbine based on doubly fed induction generator using indirect field- oriented control with fuzzy logic controllers for performance optimization. Energy Sci Eng. 2018;6:408–423. https://doi.org/10.1002/ese3.215

Zhang, F., Tong, T., and Liu, H. 2017. Design and analysis of 50KW dual-stator brushless doubly-fed generator for wind turbine. In *2017 20th International Conference on Electrical Machines and Systems (ICEMS)* (pp. 1-5). IEEE.

APPENDICES

APPENDIX 1: Matlab file for the simulation

Appendix 1: Matlab file for the simulation

```
% Parameters
clc;

% Grid
Vs = sqrt(2)*690/sqrt(3);
F = 50;     % stator frenquency
ws =2*pi*F;     %speed of stator flux
Fs = Vs/ws;     %rated stator flux(wb)

%Machine parameters
Ps = 1.5e6;     %stator rated power
Rs = 0.012;               % Stator resistance (ohm)
Rr = 0.021;               % Rotor resistance referred to stator (ohm)
Ls = 0.0137;              % Stator inductance (H)
Lr =  0.0136;              % Rotor inductance (H)
M =  0.0135;
sigma = 1-M^2/(Ls*Lr);      % Leakage Coefficient
Gp = -1.5*M*Vs/Ls;          % stator power gains
Gq = Gp;
Qc = Vs*Vs/(ws*Ls);         %reactive power compensation

p = 2;          % number of pair pole
smax = 1/3;    % maximum slip
u = 1/3;        % turn ratio

% matrices of induction generator
A = [Rs 0 0 0; 0 Rs 0 0; 0 0 Rr 0; 0 0 0 Rr];
B = [Ls 0 M 0; 0 Ls 0 M; M 0 Lr 0; 0 M 0 Lr];
C = [0 -Ls 0 -M; Ls 0 M 0; 0 -M 0 -Lr; M 0 Lr 0];
D = [0 0 0 0; 0 0 0 0; 0 M 0 Lr; -M 0 -Lr 0];

% PI controllers gains

tau_i = 0.1;
tau_p = 2.5218e-06;
% currents loops
kp_i = sigma*Lr/tau_i;
ki_i = Rr/tau_i;
% power loops
kp_P = (sigma*Lr*Ls/(M*Vs))/(tau_p);
 ki_P = (Rr*Ls/(M*Vs))/(tau_p);
% FLC controllers gains
% current loops
Ge_i = 3e-4;
Gde_i = 3e-3;
Gu_i = 13;
% power loops
```

```
Ge_p = 4.8e-7;
Gde_p = 5.6e-6;
Gu_p = 1.5e5;
```

CURRICULUM VITAE

Personal Information

Name and Surname : Kanadid ABDI ISMAN

Education

MSc	Çankırı Karatekin University Graduate School of Natural and Applied Sciences Department of Electrical and Electronics Engineering	2022-present
Undergraduate	Djibouti University Faculty of Technology Department of Electrical Engineering	2014-2018

Work Experience

Year	Institution	Position
02-2017-03-2017	Doraleh Container Terminal (DCT), Department of Electric	Traineer.
04-2018-07-2018	Doraleh Container Terminal (DCT), Department of Electric	Traineer.